Large heterogeneity of mitochondrial DNA transcription and initiation of replication exposed by single-cell imaging

Laurent Chatre and Miria Ricchetti*

Institut Pasteur, Unité de Génétique Moléculaire des Levures, CNRS UMR 3525, 25 rue du Dr. Roux, 75724 Paris, France

*Author for correspondence (mricch@pasteur.fr).

Accepted 19 November 2012
Journal of Cell Science 126, 914–926

doi: 10.1242/jcs.114322

Summary

Mitochondrial DNA (mtDNA) replication and transcription are crucial for cell function, but these processes are poorly understood at the single-cell level. We describe a novel fluorescence *in situ* hybridization protocol, called mTRIP (mitochondrial transcription and replication imaging protocol), that reveals simultaneously mtDNA and RNA, and that can also be coupled to immunofluorescence for *in situ* protein examination. mTRIP reveals mitochondrial structures engaged in initiation of DNA replication by identification of a specific sequence in the regulatory D-loop, as well as unique transcription profiles in single human cells. We observe and quantify at least three classes of mitochondrial structures: (i) replication initiation active and transcript-positive (Ia-Tp); (ii) replication initiation silent and transcript-positive (Is-Tp); and (iii) replication initiation silent and transcript-negative (Is-Tn). Thus, individual mitochondria are dramatically heterogeneous within the same cell. Moreover, mTRIP exposes a mosaic of distinct nucleic acid patterns in the D-loop, including H-strand versus L-strand transcripts, and uncoupled rRNA transcription and mtDNA initiation of replication, which might have functional consequences in the regulation of the mtDNA. Finally, mTRIP identifies altered mtDNA processing in cells with unbalanced mtDNA content and function, including in human mitochondrial disorders. Thus, mTRIP reveals qualitative and quantitative alterations that provide additional tools for elucidating the dynamics of mtDNA processing in single cells and mitochondrial dysfunction in diseases.

Key words: DNA replication, FISH, Imaging, Mitochondrial DNA, Mitochondrial disease, Transcription

Introduction

Mitochondria are ATP-producing organelles whose function is directed not only by the nuclear genome but also by their own genome. Each mitochondrion carries several copies of a circular double-stranded DNA that is replicated and transcribed autonomously in the organelle (Bonawitz et al., 2006; Falkenberg et al., 2007; Scarpulla, 2008). Mitochondrial DNA (mtDNA) is arranged in nucleoprotein complexes, nucleoids, that include factors involved in replication and transcription as well as structural proteins required for mitochondrial maintenance (Chen and Butow, 2005; Spelbrink, 2010). These proteins include DNA polymerase γ (Polγ), the enzyme responsible for replication of mtDNA, and TFAM (also known as mtTFA), a protein implicated both in transcription of and in binding to the mtDNA, and whose levels are correlated with those of mtDNA (Falkenberg et al., 2007; Poulton et al., 1994; Shutt et al., 2010). TFAM has been recently found to act more as a transcription activator than as a core component of the transcription machinery *in vitro* (Shutt et al., 2010). Human mtDNA, a 16.5 kbp molecule, is organized with two rRNA, 22 tRNAs, and 13 protein-coding genes that are transcribed from the (heavy) H-strand (12 mRNA, two rRNA and 14 tRNAs) and from the (light) L-strand (one mRNA for *ND6*, and eight tRNAs) with production of polycistronic precursor RNAs. These primary transcripts are processed to produce the individual mRNA, rRNA and tRNA molecules (Ojala et al., 1981).

The prevalent view of mtDNA replication is that DNA synthesis starts from origin O_H where the nascent H strand frequently terminates 700 bp downstream giving rise to the 7S DNA, which produces a characteristic triple stranded structure, the D-loop (Chang and Clayton, 1985; Clayton, 1991). When leading strand synthesis has reached two thirds of the genome, it exposes another major origin, the origin of L-strand DNA replication (O_L), and lagging-strand DNA synthesis then initiates in the opposite direction. However, coupled O_H and O_L strand DNA synthesis has been described in only a subset of mtDNA molecules (Holt et al., 2000) suggesting that this model is not fully elucidated. Mitochondria display a variety of shapes ranging from highly interconnected tubular structures to individual small spherical units. These structures, which are highly dynamic, are regulated by mitochondrial fusion and fission, and they vary during cell growth (Chan, 2006; Lee et al., 2007; Mitra et al., 2009). Whether these different structures are related to the processing of mtDNA (transcription and replication) needs clarification.

The processing of mitochondrial DNA has been intensively analysed with biochemical approaches (reviewed by Falkenberg et al., 2007; Scarpulla, 2008) which essentially examined global cellular and mitochondrial populations. However, little is known about the dynamics and the regulation of mtDNA transcription and replication in a single cell, as well as the implication of these

processes in cell function. Indeed, currently available fluorescence *in situ* hybridization (FISH) tools including recent improvements (Alán et al., 2010; Ozawa et al., 2007), are not fit to identify mitochondria engaged in DNA replication, and to discriminate distinct transcription profiles of the organelles. Conversely, incorporation of bromodeoxyuridine (BrdU) may label a large fraction of organelles (Echave et al., 2009), cumulating replication events that started at different times, and thereby limiting the informative potential on mtDNA replication dynamics within the mitochondrial population. Importantly, higher resolution studies have recently shown that replication of mtDNA occurs only in a subset of nucleoids (Kukat et al., 2011), underscoring the need of understanding the properties of mitochondrial replication dynamics in single cells. In this context, recent approaches based on super-resolution imaging involving mitochondrial proteins provided insightful information on the organization of nucleoids (Brown et al., 2011; Kukat et al., 2011). In spite of these advancements, and although sequential RNA and DNA labelling (Masny et al., 2010), as well as labelling of either RNA or DNA, and proteins (Arabi et al., 2005; de Planell-Saguer et al., 2010) have been performed, immunofluorescence is actually not directly coupled to FISH to simultaneously allowing the triple detection of proteins and mitochondrial DNA and RNA. Thus, proteins of interest can be hardly monitored during mtDNA transcription and replication. As a consequence, it remains unclear how mtDNA processing is coordinated among the many organelles present in each cell and to what extent this process is deregulated during disease.

Using a novel imaging protocol based on FISH, we identify mitochondrial subpopulations engaged in the initiation of mtDNA replication and in RNA processing, and assess their dynamics in single cells. Our findings reveal significant heterogeneities within single cells that have been missed previously, and show that these functions are altered upon mitochondrial dysfunction, including in diseases.

Results

mTRIP reveals heterogeneity in mitochondrial transcription

To gain insight into the dynamics of mtDNA and mtRNA within the organelle, we developed a novel protocol that labels simultaneously mtDNA and mtRNA in cells by improved FISH, and performed 3D confocal acquisitions. This approach, called Mitochondrial Transcription and Replication Imaging Protocol (mTRIP) is a combination of DNA FISH and RNA FISH techniques, and it limits the use of potentially damaging agents for macromolecules. Moreover, in contrast to other protocols, proteins are not destroyed during this treatment, as evidenced by epitope conservation of tested mitochondrial proteins during permeabilization and incubation with formamide (steps 1+2), denaturation in formamide (step 3), and the complete mTRIP procedure, Fig. 1A–D. Hence, FISH can be coupled to immunofluorescence, and it is possible to quantitatively monitor mitochondrial DNA, RNA and proteins simultaneously. The mitochondrial porin VDAC is frequently used for assessing the mitochondrial mass (Acquaviva et al., 2005), but its presence elsewhere than in mitochondria (De Pinto et al., 2010, see also supplementary material Fig. S1) led us to use TOM22 instead (Fig. 1E). TOM22, is a subunit of the mitochondrial outer membrane translocase (Yano et al., 2000) which is uniformly distributed in mitochondria, and was previously used as an indicator of mitochondrial mass (Latil et al., 2012). In this context, mitochondria are visualised as individual units or structured in the interconnected mitochondrial network. Co-labelling of mTRIP probes with TOM22 immunofluorescence was performed in this study to assess the distribution of FISH labelling in mitochondria.

We observed that mTOT, a mixture of 14 probes that cover the entire mitochondrial genome (Table 1; supplementary material Fig. S2, Table S2) labelled only a fraction of the mitochondrial network (TOM22 immunostaining) in human cells (Fig. 1F). Partial labelling of mitochondria was expected since mtDNA is normally present only in nucleoids, and mTOT indeed marked small structures within the mitochondrial mass, likely nucleoids. However, large portions of the mitochondrial network and entire TOM22-positive areas were not labelled with mTOT (mTOT/TOM22 colocalization is 23.99±1.73%), suggesting that not all nucleoids were marked with mTOT (see also below, co-labelling with nucleoid markers). Treatment of cells with either DNaseI, RNaseA or RNaseH, and combinations of these specific nucleases before hybridization with the mTOT probes showed that labelling was specific essentially for RNA molecules (Fig. 1G,H; supplementary material Fig. S3). Higher intensity of fluorescence was observed in the presence of RNaseH (1.4-fold), suggesting that removal of the RNA moiety from RNA/DNA hybrids renders DNA available for pairing with fluorescent probes. These hybrids probably correspond to transcripts bound to their DNA template. Treatment with RNaseH, then with DNaseI, restored fluorescence levels of untreated cells (Fig. 1G,H), confirming that the DNA portion of RNA/DNA hybrids does pair with the fluorescent probe, after disruption of the RNA moiety. The latter observation, and the apparent absence of effect of DNaseI treatment indicate that mtDNA is available in limited amounts for mTRIP, at least in the double-strand conformation. Treatment with proteinase K prior to mTRIP resulted in a large increase in the signal (154% for mTOT, 206% for mTRANS and 202% for mREP, Fig. 1I,J; the last two probes recognize RNA and DNA, respectively, see below) compared with untreated cells, indicating that some mtRNA and mtDNA were inaccessible to the probes because they could be bound to, or masked by proteins. In spite of this increase in signal intensity, proteinase K treatment was avoided here because mTRIP was frequently coupled to immunofluorescence for the detection of proteins.

We then performed mTRIP with each of the 14 probes defined as mTOT to examine mitochondrial transcription. Interestingly, we observed that each probe recognized a specific subset of structures (Fig. 2A), and that not only the intensity but also the distribution of the labelling varied as a function of the mtDNA region tested. Moreover, some probes (e.g. 1–4) essentially displayed a diffused labelling, whereas other probes also (e.g. 5 and 6) or prevalently (e.g. 9–12) labelled distinct foci. The foci size and number is heterogeneous, although the most intense foci on each sample are relatively constant in number (20.88±1.38 and 23.55±0.5 for probes 9 and 11, respectively). These data suggest that only a fraction of mitochondrial structures carries detectable amounts of the target nucleic acid, and that mitochondria may not be functionally equivalent in activity. Treatment with DNaseI or RNaseA showed that all of the probes recognized essentially RNA targets, with the exception of probes 4, 8 and 13, which also recognized DNA (Fig. 2B). The prevalent transcript labelled by mTRIP is 16S rRNA, which was confirmed as the most abundant mitochondrial transcript by RT-qPCR (supplementary material Fig. S4A). RT-qPCR also showed that

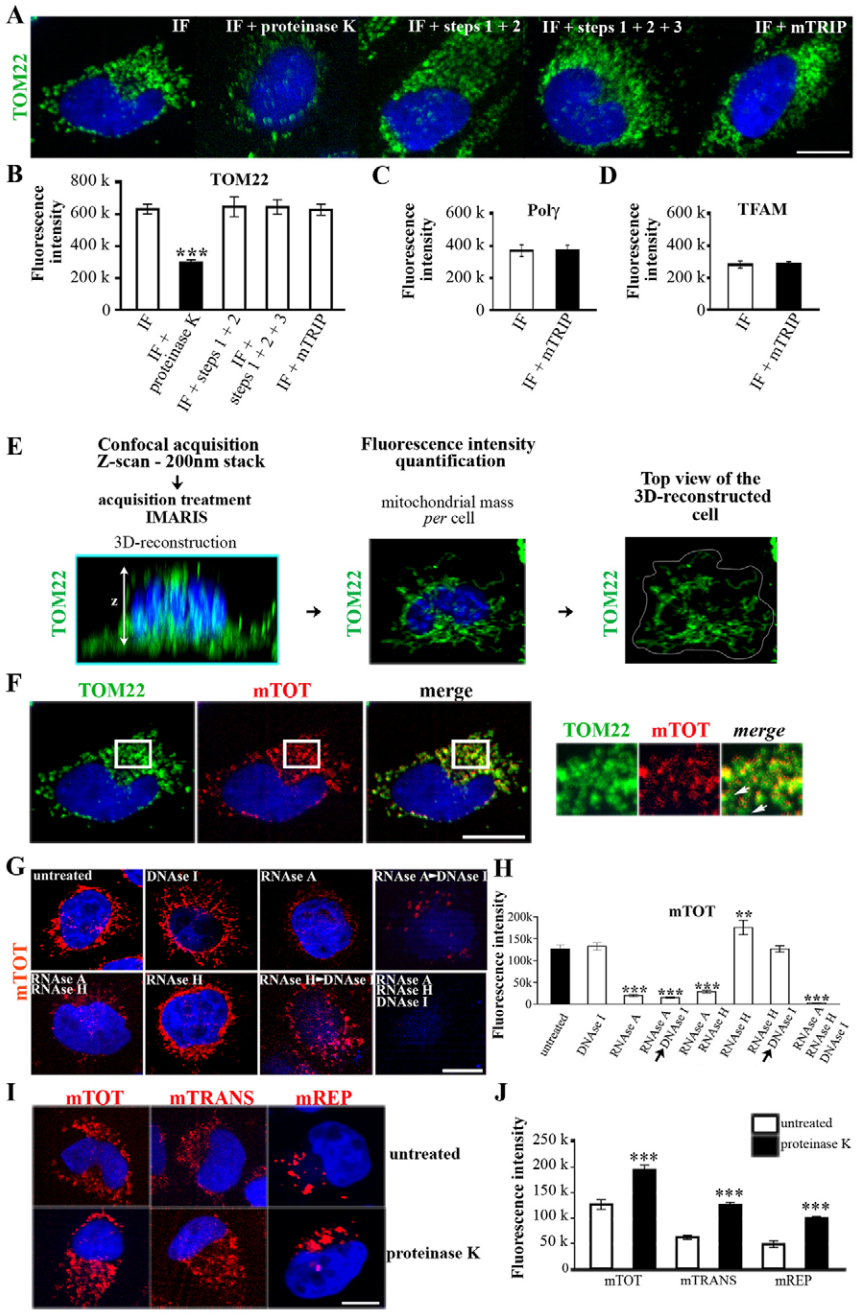

Fig. 1. Efficiency and characteristics of mTRIP labelling. (**A–D**) Epitope conservation during mTRIP treatment for relevant antibodies used in this study. (A) Anti-TOM22 immunostaining and (B) fluorescence intensity quantification of HeLa cells treated as indicated, or untreated, before immunolabelling. Steps 1+2, permeabilization+incubation with 50% formamide; step 3, denaturation in 70% formamide; mTRIP, complete procedure. A mild proteinase K treatment (5 min at 37°C), which does not completely degrade proteins, was used as a control for protein degradation. Fluorescence intensity quantification of (C) Polγ and (D) TFAM immunostaining of HeLa cells pre-treated with the complete mTRIP protocol, or untreated. IF, immunofluorescence. (**E**) Scheme for the 3D analysis of cells immunolabelled with TOM22. The same procedure was used for mTRIP labelling (DNA probes). (**F**) 3D-reconstruction of a HeLa cell shows the mitochondrial fraction labelled with the mtDNA probe mix mTOT (red). The mitochondrial network is labelled with TOM22 by immunofluorescence (green) and the nucleus with Hoechst (blue). On the right, 2.5× magnification of the indicated area; white arrows, mTOT-free areas. (**G**) 3D-reconstructed cells labelled with mTOT probe (red) and (**H**) fluorescence intensity quantification, with or without nuclease treatment (specified at the top of each panel; arrows indicate that the second nuclease was added after a 1 h incubation with the first nuclease). The mitochondrial network in cells labelled with mTRIP in the presence of nucleases is shown in supplementary material Fig. S3. (**I**) 3D-reconstructed cells labelled with mTOT in the presence or absence of proteinase K treatment. The other relevant FISH probes used in this work (mTRANS and mREP) were also tested. (**J**) Fluorescence intensity quantification of mTOT, mTRANS, and mREP, with or without proteinase K treatment. Student's *t*-test, compared with untreated cells (in panel B compared with IF). Scale bars: 10 µm.

transcript levels of mitochondrial genes were generally consistent with RNA levels identified by mTRIP (supplementary material Fig. S4A,B, Table S2), thus validating the FISH data.

To determine the relative proportions of each of the transcripts within the mitochondria, we co-labelled TOM22 by immunofluorescence with the individual probes by FISH. This analysis confirmed that 16S rRNA was present in a larger fraction of the mitochondrial network (supplementary material Fig. S5A,B), as well as it was the highest in signal intensity correlating with TOM22 labelling (supplementary material Fig. S5C), compared with the other transcripts. In addition, experiments of co-labelling with two or more probes indicated that mTRIP labels both processed and unprocessed polycistronic transcripts. Indeed, the extensive colocalization (Fig. 3A,B) and the high levels of mTRIP labelling with probe 2 and probe 3, as well as with probe 7 and probe 9 (Fig. 3D,E), suggest that the RNAs recognized by these probe pairs, which label successive genes on the H-strand, are located on the same submitochondrial structures, and might thus correspond to unprocessed transcripts. Conversely, probe 3 and probe 4 (Fig. 3A,B), as well as probe 9 and probe 10 (Fig. 3D,E), which also label successive genes on the H-strand, are essentially located on different submitochondrial structures, and likely correspond to distinct processed transcripts. In colocalization experiments, although confocal fluorescence microscopy does not allow defining whether the target nucleic acids are located on the same molecules (the limit set on the spatial

Table 1. Coordinates of the probes

Probe	Start	End	Size
1	1905	2866	961
2	2842	3554	712
3	3451	4825	1374
4	4805	6129	1324
5	6032	7420	1388
6	7400	8518	1118
7	8498	9824	1326
8	9804	11190	1386
9	11107	12618	1511
10	12513	13517	1004
11	13416	14836	1420
12	14805	16055	1250
13	15778	600	1376
14	501	2024	1523
13-1	16034	521	1041
ND6	14658	14180	479
PH1–2	546	746	200
PL-OH	225	425	200
7S	16366	16566	200
mREP	446	544	98
mTRANS	probes 1, 6, 11		
mTOT	probes 1 to 14		

The start and end points of probes used for FISH experiments are given on the mitochondrial DNA (NC_012920, GenBank, was used as reference; human mitochondrial genome size is 16,568). Individual probes are indicated with their coordinates and size (in nt). Mixes of more than one probe and their composition are also indicated. All probes are oriented in the direction of transcription of the H-strand, with the exception of probe ND6 that is in the inverse orientation (transcription on the L-strand).

resolution by diffraction of the light is 200 nm (Isobe et al., 2010), these data nevertheless show that the nucleic acids co-labelled by the selected probes are spatially and quantitatively linked. Interestingly, these co-labelling experiments also showed that about half of mitochondrial entities labelled with probe 14, which recognizes *12S* present at beginning of H-strand, colocalize with probe 12, which recognizes *CytB* present at end of H-strand, indicating that these mitochondria might contain the complete H-strand transcript (Fig. 3D–F).

To analyse further mitochondrial transcripts, a new mixture of probes was used (mTRANS: probes 1, 6 and 11) that are distributed evenly along the circular genome (supplementary material Fig. S6A). These probes label 16SrRNAs and several tRNAs and mRNAs, and they do not recognize regions involved in the initiation of DNA replication (see below). FISH experiments with mTRANS, in the absence or presence of nucleases, confirmed that this probe set detects only RNA (see below). The nucleoid markers TFAM and Polγ label submitochondrial structures, as shown in supplementary material Fig. S6B,C. Extensive colocalization between immunostaining of either Polγ or TFAM and mTRANS (supplementary material Fig. S6D) indicated that transcripts detected by this probe mix were mostly confined to labelled mitochondrial nucleoids, as suggested above. The different levels of colocalization between FISH probes and nucleoid markers might be linked to heterogeneity of nucleoids (DNA and protein content).

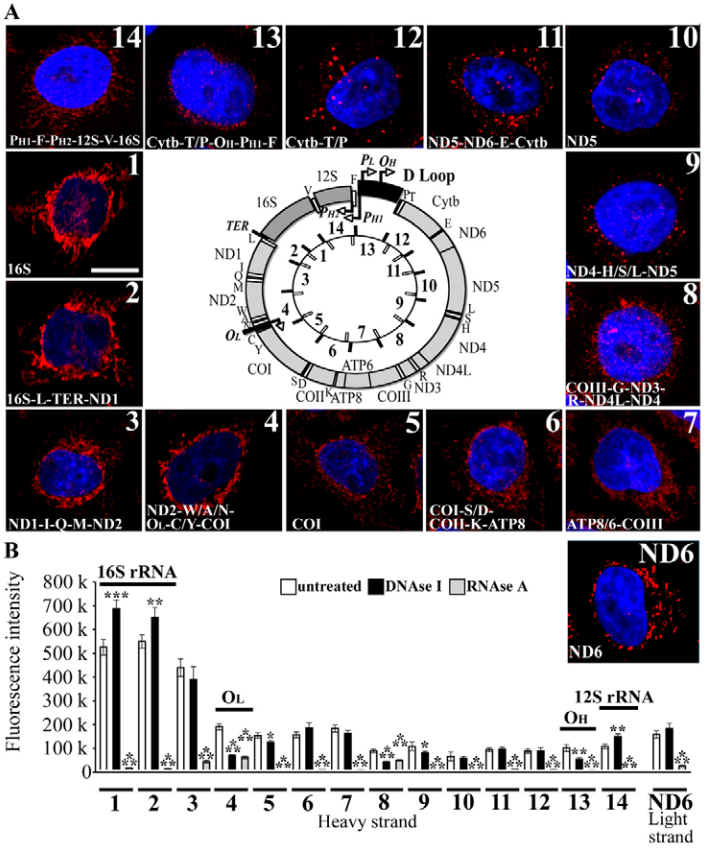

Fig. 2. Heterogeneity of mitochondrial transcripts in single cells. (**A**) mTRIP of HeLa cells with 14 individual mtDNA probes (red), each covering a portion of the entire mitochondrial genome. Nuclei (blue) are labelled with Hoechst. The probe name, and the mitochondrial gene(s) covered by the probe are indicated at the top and bottom of each panel, respectively. The central panel is a scheme of the mitochondrial genome (external circle) and of single genes within, to scale. tRNA genes are indicated with the corresponding letter. All genes are located on the H-strand, with the exception of *ND6*, located on the L-strand. rRNAs (*16S* and *12S*) are in dark grey and slightly shifted out of the circle. The D-loop region [containing the H-strand origin of replication (O_H) and promoters of both H and L strands (P_{H1}–P_{H2}, and P_L, respectively)] is shown in black and shifted out of the circle. The inner circle shows the positions of individual probes (see coordinates, Table 1). The 14 individual probes cumulatively cover the complete mitochondrial genome. Labelling with probe ND6 (covers the *ND6* gene located on the L-strand) is also shown. Scale bar: 10 µm. (**B**) Fluorescence intensity quantification of 3D-reconstructed HeLa cells labelled with each of the 14 mtDNA probes and with probe ND6 indicated on the *x*-axis, untreated or treated with either DNaseI and RNaseA. For each probe, the Student's *t*-test was performed for nuclease-treated versus untreated cells. For most probes, labelling decreases dramatically or is lost after RNaseA treatment, indicating that the targets are essentially RNA molecules. DNaseI treatment of probes 4, 8 and 13 results in partial or total reduction of the label, indicating that they target also mtDNA. Probes 4 and 13 cover replication origins (O_L and O_H, respectively).

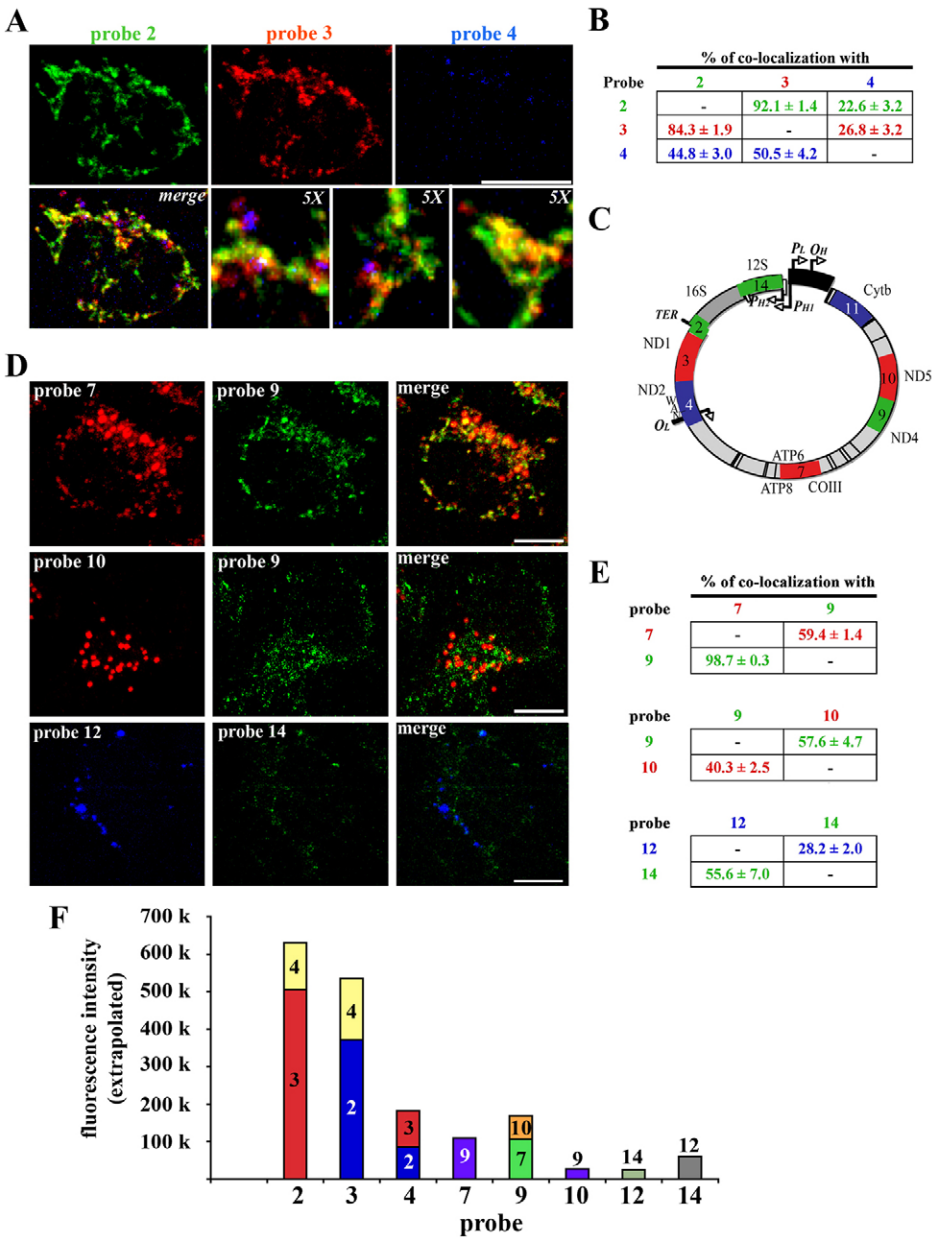

Fig. 3. Co-labelling with several mtDNA probes. (**A**) 3D-reconstructed HeLa cells co-labelled with probes 2 (green) 3 (red) and 4 (blue), upper panels; and a merged image with 5× magnification of three distinct regions (lower panels). The probe used is indicated above. (**B**) Percentage of colocalization of the various probes. The extensive colocalization between probe 2 and probe 3, and the high levels of mTRIP labelling with both probes, are compatible with the possibility that probe 3 also targets non-terminated rRNA transcripts. Indeed, when *ND1* is targeted by the specific probe ND1, the intensity of mTRIP signal is comparable to the other mitochondrial mRNAs rather than to 16sRNA (see supplementary material Fig. S4C, Table S2). Percentages of co-labelling also depend on the total intensity of fluorescence specific to each probe, thus, percentages of co-labelling between probe pairs (as probes 2 versus 3 compared with probes 3 versus 2) might be different. (**C**) Scheme of the position of probes on the mitochondrial genome; the probe is reported in colour and the probe number is indicated. (**D**) 3D-reconstructed cells co-labelled with probes 7 (red) and 9 (green), upper panels; with probes 10 (red) and 9 (green), middle panels; and with probes 12 (blue) and 14 (green), lower panels. Merges are shown in the right-hand panels. (**E**) Percentage of colocalization of indicated probes. High levels of colocalization appear for probes 7 and 9. In contrast, the rare colocalization of transcripts targeted by probes 9 and 10 reveals that most of this transcript pair are not present in the same mitochondrial substructures. (**F**) Summary of colocalization results. Probes are indicated on the *x*-axis. The *y*-axis reports the intensity of co-labelling with the probe(s) indicated on the segment(s) of the column. These *y*-axis values represent the percentage of co-labelling multiplied by the fluorescence intensity signal of the tested probe. These colocalization experiments strongly suggest that transcripts labelled by mTRIP probes represent both unprocessed RNA molecules and processed transcripts. Scale bars: 10 µm.

mTRIP exposes mtDNA initiation of replication

We observed above that three probes (4, 8 and 13) detect not only RNA but also DNA. Interestingly, probes 13 and 4 include the regions of initiation of replication of the H- and the L-strand, respectively, suggesting that these probes detect DNA regions engaged in the initiation of replication. Probe 8 includes the *ND4* region, where an additional origin of replication for the L-strand (O_{ALT}) has been reported using atomic force microscopy (Brown et al., 2005), and which is expected to be activated less frequently than the two major origins. These three origins are distributed evenly on the mitochondrial genome, as schematized in Fig. 4A. Labelling with probe mREP, which is a subset of probe 13 (Fig. 4B,C), was DNaseI-sensitive and RNaseA- and RNaseH-resistant (Fig. 4D) indicating that this probe labels DNA specifically. Conversely, Fig. 4D shows that probe mTRANS labels mRNA specifically.

Since the DNA region recognized by mREP is present in the genome of all mitochondria, we reasoned that the local DNA structure, likely the adjacent O_H origin of replication, rendered it accessible to the probe. To verify this point, we assessed whether mREP is associated with nucleoids that contain factors involved in DNA replication and transcription. mREP labelling coupled to immunofluorescence with Polγ or TFAM showed that this was the case (74.4±2.5% colocalization of mREP with Polγ, and 71.7±1.5% with TFAM, Fig. 4E), and also that most of the mREP *foci* were preferentially localized to Polγ and TFAM-rich areas (Fig. 4F).

To assess whether mREP was associated with mtDNA replication, we checked BrdU incorporation, an indicator of DNA replication, in mitochondria. Proliferating cells were treated with 10 µM BrdU for 30 min, 90 min, 3 h, 6 h, 9 h and

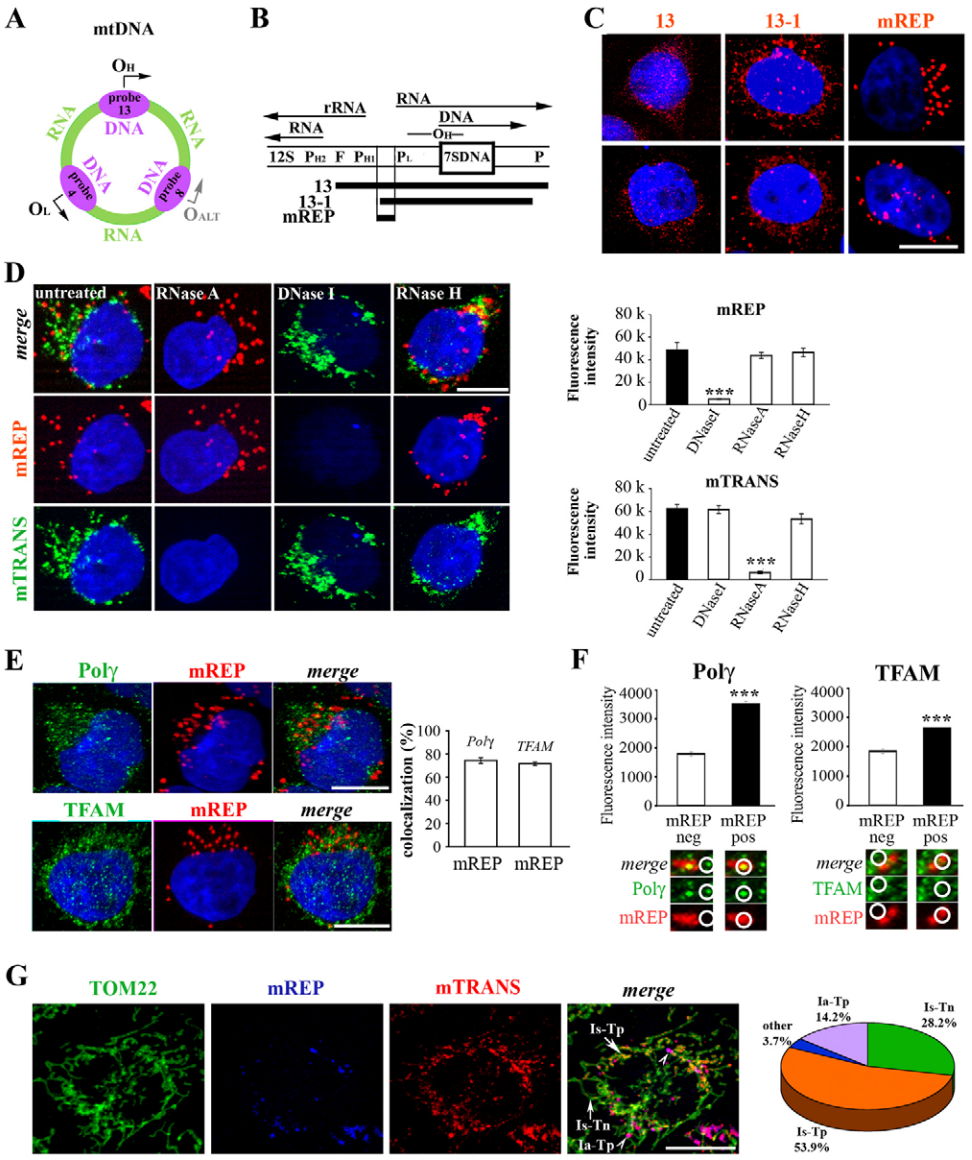

Fig. 4. Identification of mtDNA initiation of replication. (**A**) Schematic representation of nucleic acids detected with probes 1 to 14, as from Fig. 2B. In addition to RNA labelling, DNA labelling is observed on three regions (not to scale); probes 13 and 4 include origins O_H and O_L, respectively; probe 8 includes a third origin, O_{ALT}, on the L-strand (Brown et al., 2005). The direction of DNA synthesis is indicated with an arrow. A grey arrow represents a less frequently activated origin. (**B**) Characterization of the O_H region. The region recognized by each probe is shown; main genetic elements are also shown (F=tRNA^{Phe}; 12S=12S rRNA, P=tRNA^{Pro}). Only probe mREP covers a region that is essentially not transcribed. (**C**) 3D-reconstructed cells labelled with the indicated probes (red) in the O_H region; nucleus in blue (Hoechst). mREP labelling consists of 21.55±1.27 foci/cell (n=30 cells). (**D**) 3D-reconstructed cells labelled with mREP (red) and mTRANS (green) probes, with or without nuclease treatments (left-hand panels), and fluorescence intensity quantification (right-hand panels); Student's t-test for nuclease-treated versus untreated cells. (**E**) mTRIP-coupled immunofluorescence with mREP (red) and either anti-Polγ (green) or anti-TFAM (green), upper and lower panels, respectively. mREP foci appear relatively large and might include more than one nucleoid marker [nucleoids are about 70 nm in size (Brown et al., 2011; Chen and Butow, 2005; Kukat et al., 2011)]. On the right, colocalization (%) of mREP with anti-Polγ or anti-TFAM. Note that a fraction of mREP foci does not colocalize with one or the other nucleoid markers. (**F**) Fluorescence intensity quantification of mREP-positive (pos) and mREP-negative (neg) Polγ- or TFAM-labelled areas. Examples of respective areas are shown, circled, below the x-axis; n=300, Student's t-test, mREP-negative versus mREP-positive. (**G**) Co-labelling with mTRANS (red) and mREP (blue) probes, and TOM22 immunofluorescence (green) shows mitochondrial initiation of replication, transcription and mitochondrial network simultaneously. In the merged image, mREP essentially colocalizes with mTRANS (purple, arrowheads; Ia-Tp, replication initiation active and transcript-positive); independent mTRANS labelling is detected (orange, arrow; Is-Tp, replication initiation silent and transcript-positive). Replication initiation silent and transcript-negative mitochondrial structures are also observed (green, vertical arrow, Is-Tn). Fluorescence intensity quantification is reported in the text. Scale bars: 10 µm. Right-hand panel: pie chart representation of the different mitochondrial structures, with the percentages indicated. Values are calculated taking into account the extent of co-labelling between mREP and mTRANS, and the percentage of the distinct labelling of each probe within the mitochondrial mass (TOM22). Other labelling, essentially mREP-positive and mTRANS-negative, which might represent replication initiation active and transcript-negative (Ia-Tn) structures, is also detected but is not considered further given the limited signal.

18 h prior to FISH labelling (supplementary material Fig. S7A). Long-time exposure of cells to BrdU (i.e. 18–24 h) is generally used to detect full mtDNA replication (Echave et al., 2009). Short-time exposure to the drug was tested here to assess the kinetics of mtDNA replication, and early replication events. We observed that in spite of the BrdU labelling increases with the time of treatment, as expected because of the accumulation of labelled mitochondrial and nuclear DNA (nDNA), the extent of mREP/BrdU colocalization remains relatively constant, at least until 9 h of treatment (supplementary material Fig. S7B). This result indicates that mREP does not co-label mitochondrial structures carrying progressively longer mtDNA chains but rather a specific subset of mtDNA replication events at each time point, which are compatible with replication initiation events. Most mREP-positive structures are not labelled with BrdU, compatibly with an open mtDNA structure that has not incorporated BrdU or that has incorporated BrdU below detection levels (see schema in supplementary material Fig. S7C). Interestingly, after 18 h treatment, at constant mREP labelling, 80.4±2% of mREP positive structures colocalize with BrdU, indicating that under these conditions most of the open mtDNA structure located nearby the replication origin are productively engaged in initiation of mtDNA replication. As for above, the remaining 19.6% of mREP foci are compatible with an open mtDNA structure that is engaged in replication where little or no DNA synthesis has occurred.

Importantly, at all time points, mREP is detected in only a subset of BrdU-positive foci, i.e. a subset of structures engaged in DNA replication, in agreement with the notion that this probe does not detect extensive or completed replication, but rather the initiation of DNA replication. In this context, the intensity of BrdU labelling, evaluated after 18 h of BrdU treatment and taking into account BrdU-positive areas located extranuclearly, was lower in mREP-positive compared with mREP-negative areas (see isolated mitochondria located outside the nuclear region, and quantification, supplementary material Fig. S7D), in agreement with the limited incorporation of a nucleotide analogue at the beginning of replication of the mitochondrial genome. Finally, we observed that mREP signal increased when the mtDNA content was reduced, and returned to control values when the original mtDNA content was restored (treatment with low levels of H_2O_2, supplementary material Fig. S7E). Taken together, these results, and the unique characteristics of the region of the mtDNA recognized by mREP, support the notion that mREP marks initiation of replication.

Whether DNA synthesis detected by mREP proceeds from O_H until the end of the H-strand, or terminates earlier, leading to the formation of the 7S strand and thereby of the D-loop (Chang and Clayton, 1985; Clayton, 1991), was not resolved by FISH labelling alone. To elucidate this point, we compared endogenous levels of mtDNA and of 7S DNA detected by real-time qPCR, as described (Antes et al., 2010) in cells with affected levels of mtDNA (treatment with low levels of H_2O_2, see above). We found that the variations observed in the mtDNA content after exposure to H_2O_2, evaluated in the 12S region, and associated with changes in mREP levels (supplementary material Fig. S7E) are compatible with variations of the mtDNA and not of 7S DNA (supplementary material Fig. S7F). Thus, although mREP may label both the productive and the abortive initiation of mtDNA replication (formation of the D-loop), variations in mREP are compatible with productive replication of the mtDNA rather than with the formation of the D-loop.

Three distinct classes of mitochondrial structures engaged or not in initiation of DNA replication and/or in transcription are detected by mTRIP

To assess the fraction and the distribution of mtDNA processing activities within the mitochondrial network we performed co-labelling with mREP, mTRANS, and TOM22 (Fig. 4G). Notably, 58.9±2.7% and 12.9%±1.3% of the mitochondrial mass (TOM22 immunolabelling) co-labelled with mTRANS and mREP, respectively, revealing that most mitochondrial structures carry detectable transcripts (red label, Fig. 4G), whereas only a small fraction of these structures is engaged in initiation of mtDNA replication (blue label, Fig. 4G). A significant fraction of the mitochondria were not labelled with either probe indicating that either they are not involved in the transcription of the tested genes and/or in the replication of mtDNA, or that the levels of the target molecules are not detectable with this approach (replication initiation silent and transcript-negative mitochondrial structures, Is-Tn, or mREP-negative and mTRANS-negative, green label, Fig. 4G).

Moreover, the majority (71.3±2.9%) of mitochondrial structures involved in the initiation of replication also carried mTRANS transcripts (replication initiation active and transcript-positive mitochondrial structures, Ia-Tp, or mREP-positive and mTRANS-positive, purple, labelling). On the contrary, the majority (91.5±0.8%) of mitochondrial structures that carried detectable transcripts were not involved in initiation of mtDNA replication in these cells (replication initiation silent and transcript-positive mitochondrial structures, Is-Tp, or mREP-negative and mTRANS-positive, orange, labelling). The proportion of these distinct structures within the mitochondrial network is shown on the right-hand panel in Fig. 4G. Thus, we identify at least three classes of mitochondrial structures with distinct mtDNA processing activities within a single cell.

Heterogeneous labelling of the regulatory D-loop region in mitochondria within single cells

We reasoned that since mTRIP identifies distinct mitochondrial structures within single cells according to the DNA engaged in initiation of replication and to the transcript content, it should also identify mitochondrial structures with distinct RNA and DNA labelling patterns in the regulatory region, which might be functional to the regulation of mtDNA itself. To assess this point, we performed FISH with three probes located in the D-loop region (probes PL-OH and 7S) and at promoters of the H-strand (P_{H1} and P_{H2}; probe PH1–2), see schema Fig. 5A. We performed single labelling, and colocalization experiments with two probes, in the presence and in the absence of nucleases.

Quantitative analyses of fluorescence showed that probe PL-OH, located downstream of mREP in the direction of DNA replication, and which includes the P_L and the O_H regions, labels accessible DNA structures (DNaseI-sensitive labelling, Fig. 5B,C), which might be part of the P_L transcription bubble, or of the O_H replication bubble, or of both. This last possibility is in agreement with a large set of evidences indicating that transcription from P_L is coupled to H-strand replication (Scarpulla, 2008). Probe PL-OH also labels RNA in RNA/DNA hybrids (reduction of labelling in the presence of RNaseH, Fig. 5B,C). These RNA molecules might consist of R-loops, i.e.

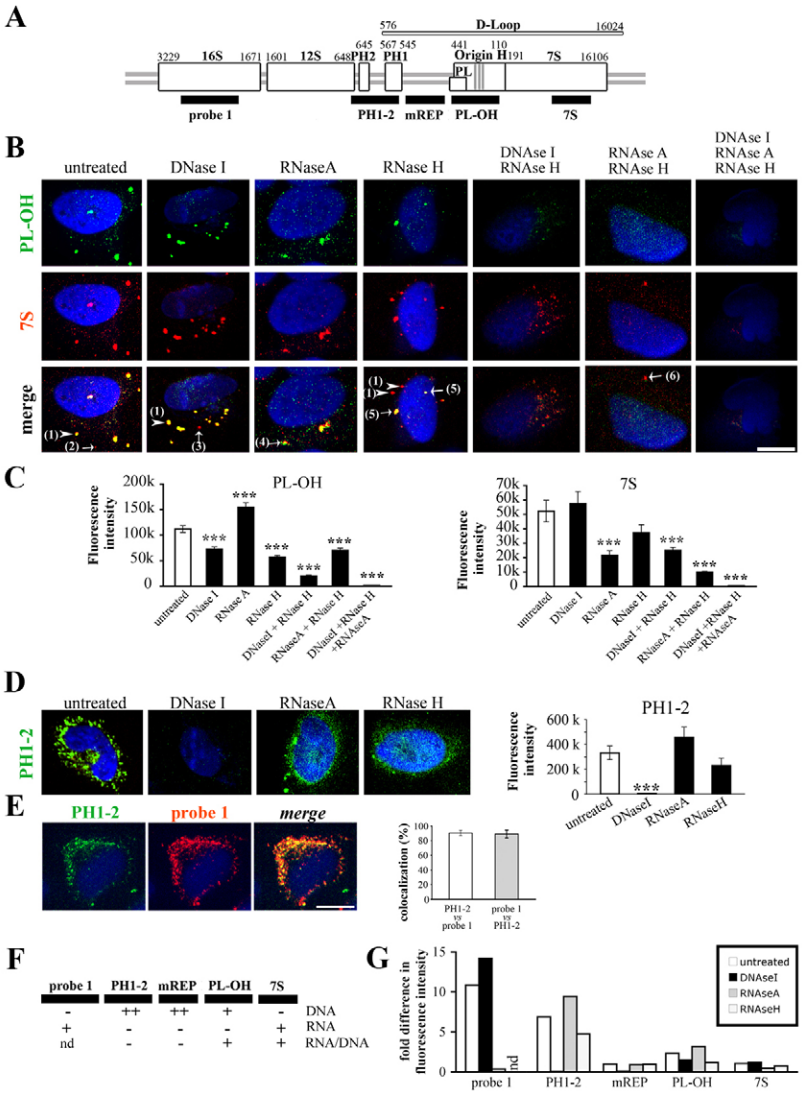

Fig. 5. Heterogeneity of mtDNA transcription and replication initiation structures in the regulatory D-loop region. (**A**) Schematic representation (not to scale) of the D-loop region of mtDNA analysed by mTRIP; key elements and coordinates in mtDNA are indicated; vertical grey bars in the O_H region represent the three CSB sites; *16S* and *12S* genes, and the 7S region are shown. mTRIP probes (horizontal black bars) are named and their position on mtDNA is indicated. (**B**) 3D-reconstruction of cells labelled with probes PL-OH or 7S; merged images are also shown. Cells were treated with the nucleases indicated above the images or untreated. In the merge panels, in addition to small foci and diffused labelling, arrowheads and arrows indicate large foci with different labelling patterns (1–6), according to the sensitivity to the various nucleases. (**C**) Fluorescence intensity quantification of probes PL-OH (left-hand panel) and 7S (right-hand panel) in the presence or absence of the indicated nucleases. (**D**) 3D-reconstruction of cells labelled with PH1–2 in the presence and in the absence of nucleases. On the right, fluorescence intensity quantification. (**E**) 3D-reconstruction of cells labelled with probe PH1–2 or probe 1; the merged image is also shown; on the right, percentages of colocalization. (**F**) Schema of detected nucleic acids (according to the sensitivity to nucleases) in the corresponding region on the scheme, including data of probe mREP from Fig. 4D (++, exclusive detection; +, detection, −, no detection; nd, not done). (**G**) Summary of intensity of fluorescence labelling with different probes in the presence or absence of nucleases, normalized to values of mREP (in the absence of nucleases). nd, not done. Scale bars: 10 µm. Student's *t*-test for nuclease-treated versus untreated cells.

the RNA primers for DNA synthesis for the O_H origin (Brown et al., 2008), present as processed as well as unprocessed molecules of various lengths, or regular L-strand transcripts, or both. Interestingly, simultaneous treatment with DNaseI and RNaseH resulted in residual labelling (19.9%±1.4%) that disappeared when cell were also treated with RNaseA (Fig. 5C). This experiment indicates that probe PL-OH also labels RNaseH-resistant RNA/DNA hybrids, which become accessible to RNaseA after the DNA moiety is removed by the action of DNaseI. This finding is in agreement with the notion that the structure of the RNA/DNA hybrids in R-loops may confer resistance to RNaseH (Brown et al., 2008). Increase in the intensity of labelling in the presence of RNaseA indicates not only that RNA is not a significant target of PL-OH but also that RNA molecules to a certain extent inhibit the labelling of other targets.

The labelling of nucleic acids appears rather different in the downstream 7S region (probe 7S). Indeed, treatment with nucleases indicates that probe 7S recognizes prevalently RNA (Fig. 5B,C). Probe 7S also targets RNA/DNA hybrids, since treatment with RNaseA did not reduce the FISH signal to background levels, and simultaneous treatment with RNaseH and RNaseA resulted in significant decrease of the signal, compared with RNaseA alone ($P=0.0013$).

More detailed information on the heterogeneity of the nucleic acids composition of the D-loop region in mitochondria was provided by the direct observation of foci. Indeed, PL-OH and 7S labelling consist of small foci with poor fluorescence intensity as well as of large foci of intense fluorescence, and distinct colocalization patterns with the other probe (arrows with numbers, Fig. 5B). Fluorescence intensity measurements in Fig. 5C take in to account all foci; large foci were separately enumerated and further examined. Analysis detailed in supplementary material Fig. S8 identifies the nucleic acid composition of several labelling patterns associated with large PL-OH and/or 7S foci, and shows the large heterogeneity of mTRIP labelling in this region. The existence of these labelling patterns, and the proportions of these events are indicative of qualitatively and quantitatively distinct mtDNA processing activities in the D-loop which occur simultaneously within single cells.

Linked nucleic acid structures in the D-loop

Although the limits of resolution of FISH do not discriminate whether labelled nucleic acids are present on the same molecules

(or on the same structures), several observations support the notion that most large PL-OH and 7S foci (patterns 1, 3–5) label related entities. Indeed, these foci appear simultaneously affected by treatment with RNaseA alone, and combined treatment with RNaseA and RNaseH (Fig. 5B; supplementary material Fig. S8A). Additionally, large PL-OH and 7S foci disappeared after simultaneous treatment with RNaseH and DNaseI (whereas treatment with DNaseI alone had essentially no effect, and treatment with RNaseH affected only PL-OH foci). This experiment indicates that RNA/DNA hybrids, at least at the level of 7S, are essential to the formation of the large structures labelled not only by probe 7S but also by probe PL-OH, thereby further supporting the notion that the nucleic acids labelled by the two probes are linked. Moreover, after treatment with two nucleases, large foci were replaced by smaller foci of variable size, which in most cases did not colocalize (Fig. 5B), indicating that, differently from large foci, the target nucleic acids are no longer present in linked structures. Importantly, nucleic acids in this regulatory region were accessible in only a limited fraction of mitochondria (co-labelling of either PL-OH or 7S with TOM22, not shown), revealing a further heterogeneity of mitochondrial structures in single cells for the PL-OH and 7S target regions.

Finally, colocalization experiments revealed that not only PL-OH colocalizes by 99.44%±0.05% with 7S, but also that mREP colocalized with 7S by 99.33%±0.07% indicating that mREP, PL-OH and 7S likely label linked, although heterogeneous, nucleic acid structure(s) (results are integrated in Fig. 5G). Conversely, only a fraction of 7S colocalizes with mREP (59.8%±2.6%), and with PL-OH (69.7%±2.7%), indicating that 7S does not label only RNA involved in the replication bubble, compatibly with labelling of L-strand transcripts. In agreement with this notion, the intensity of PL-OH labelling was 2.3-fold higher than mREP labelling (Fig. 5G).

In conclusion, probes PL-OH and 7S identify a fraction of mitochondria carrying a variety of linked structures with distinct nucleic acid composition that appear associated at different levels with O_H DNA replication and L-strand transcription and that co-exist in single cells.

mtDNA transcription dynamics in the P_H promoters region at the single cell level

On the other side of mREP, probe PH1–2, which is located in the region of promoters P_{H1} and P_{H2}, was fully sensitive to DNaseI, indicating that it labels essentially DNA (Fig. 5D). The accessible DNA in this region might result from its opening as a consequence of the nearby O_H replication bubble, or represent the P_{H1}/P_{H2} transcription bubble. The overwhelming colocalization between probe PH1–2 and probe 1, which labels 16S RNA transcribed essentially from P_{H1}, (Fig. 5E), and the elevated intensity of fluorescence observed with both probes support the second notion. Treatment with either RNaseA or RNaseH does not significantly alter the efficiency of PH1–2 labelling, although foci display a different aspect compared with untreated controls (Fig. 5D), indicating that although RNA and RNA/DNA hybrids do not appear to bind probe PH1–2, they might affect the structure of the DNA to which the probe binds. A summary of the prevalent nucleic acids detected in the regulatory region of the mtDNA is shown in Fig. 5F.

A large difference in the extent of labelling among probes located in the D-loop was noted. PH1–2 fluorescence intensity was 6.9-fold higher than mREP, and probe 1 fluorescence intensity, which marks the 16S transcript, was 10-fold higher than mREP, compatibly with robust transcription of rRNAs (Fig. 5G). Simultaneous labelling with two probes reveals that 48.73%±3.44% of mREP foci colocalize with PH1–2 foci, indicating that accessible DNAs in the two regulatory regions might be linked, although in other cases these foci do not colocalize, compatibly with the notion that transcription of rRNA can be uncoupled from the formation of the DNA structure that promotes replication in the O_H region.

Alterations in mtDNA processing in cells with perturbed mtDNA content

To assess whether mTRIP detects alterations of DNA processing in cells with mitochondrial perturbations we examined HeLa *rho*^{0} cells where mtDNA is lacking (Parfait et al., 1998), and HeLa cells treated with ethidium bromide (EtBr) for three days to reduce their mtDNA content (King and Attardi, 1996). Notably, HeLa *rho*^{0} cells contained about one third of the mitochondrial mass (TOM22 immunolabelling, Fig. 6A,C; see also supplementary material Fig. S1A,C,D) compared with regular HeLa cells, but no signal was detected with either mTRANS or mREP, confirming the absence of mtDNA transcription and initiation of replication in these cells (Fig. 6B). *Rho0* cells did not show detectable BrdU signal in extranuclear areas (Fig. 6D), as expected because of the lack of mtDNA. In contrast, cells treated with EtBr, which had a reduced mtDNA content, maintained a regular mitochondrial mass and displayed a 9.3-fold and a 5.9-fold increase in the levels of mREP and mTRANS, respectively, compared with untreated cells. High levels of transcripts were confirmed by RT-qPCR of mitochondrial *16S* rRNA and *CytB*. These data indicate that in spite of mtDNA depletion, EtBr-treated cells dramatically increased their mtDNA replication and transcription activities, likely to compensate for the low DNA content, in agreement with previous studies on transcription in these treated cells. (Seidel-Rogol and Shadel, 2002).

Finally, we analysed primary fibroblasts mutated in *RRM2B*, the p53-inducible ribonucleotide reductase subunit which is essential for mtDNA synthesis and is associated with mtDNA depletion syndrome (Bourdon et al., 2007). We found that *Rrm2b* fibroblasts in spite of a 44% reduction in the mitochondrial mass (TOM22; see also VDAC and MitoTracker® labelling; Fig. 7C,D; supplementary material Fig. S9) display a 4-fold reduction in mREP and a 3-fold reduction in mTRANS signals compared with normal fibroblasts (Fig. 7A,B). Moreover the number of foci with mREP labelling decreased from 28.44±0.96 in normal fibroblasts to 11.55±1.38 in mutant fibroblasts. Furthermore, although normal and *Rrm2b* fibroblasts maintain relatively constant mREP as well as mREP+/BrdU+ signal at increasing exposure to BrdU, the extent of both signals is dramatically reduced in mutant fibroblasts, indicating that *Rrm2b* cells carry a severely reduced fraction of mitochondrial structures engaged in initiation of mtDNA replication (Fig. 7E,F).

Taken together, the analysis of three different cell types showed that mREP and mTRANS labelling identify altered or loss of mtDNA processing, which affects mitochondrial function, thus validating mTRIP for monitoring disease states both qualitatively and quantitatively.

Discussion

Mitochondria play a crucial role in eukaryotic cells, therefore understanding the dynamics of DNA transcription and replication within the mitochondrial network, and possibly within

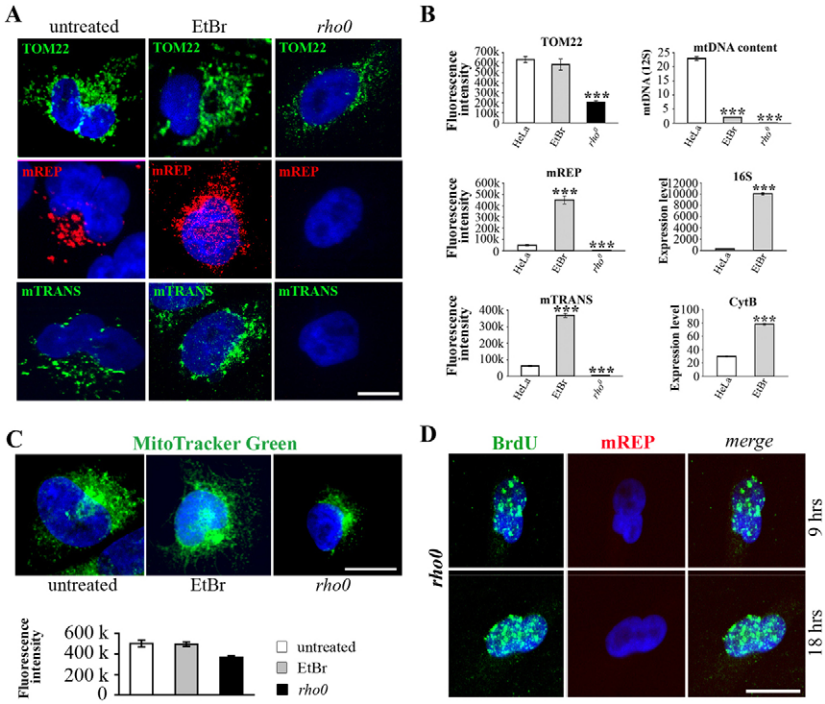

Fig. 6. mTRIP detects mtDNA processing alterations in cells with perturbed mtDNA content. (**A**) 3D-reconstructed HeLa cells analysed by mTRIP with probes mREP (red) and mTRANS (green) and by immunofluorescence with TOM22 (green). Cells were either untreated or treated with EtBr for 3 days to decrease their mtDNA content. The more diffuse mREP and mTRANS signal in these cells compared with untreated cells could be due to damaged nucleic acids in the presence of the intercalating agent. In cells treated with EtBr, fluorophores visible as red cannot be used since the excitation/emission spectra of DNA-bound EtBr are also in the red (526/605 nm). Therefore, in these experiments mREP is labelled and quantified with Atto488-dUTP, but in this figure mREP is represented in red to keep the colour code homogeneous with the other samples. HeLa *rho*^{0} cells were also analysed. (**B**) Fluorescence intensity quantification. MtDNA content of cells analysed by qPCR in the 12S region, and expression levels of 16S and CytB RNAs analysed by RT-qPCR are shown. Student's *t*-test for treated or mutated cells versus untreated cells. (**C**) Untreated, Et-Br-treated and *rho0* HeLa cells labelled with MitoTracker® Green. Lower panel: fluorescence intensity quantification. (**D**) *rho0* cells labelled with mREP and anti-BrdU after 9 h and 18 h of exposure to BrdU.

mitochondrial substructures, is important to assess mitochondrial function (Brown et al., 2011; Chen and Butow, 2005; Kukat et al., 2011; Spelbrink, 2010). We describe here a novel FISH protocol, mTRIP, which identifies an unexpected variety of mitochondrial structures and mitochondrial populations with distinct properties within single cells. These populations differ in their intracellular localization, in the relative amount of transcripts that they express, in the initiation of DNA replication, and in the intensity and type of signal in regulatory regions, indicating that mitochondria and mitochondrial structures exhibit a greater level of heterogeneity in DNA processing activities than reported previously, including mitochondrial dynamics during mtDNA synthesis (Davis and Clayton, 1996). Within the limits of resolution of this approach, which relies on confocal microscopy, and not on super-resolution microscopy (Brown et al., 2011; Kukat et al., 2011), labelling of mtDNAs and RNAs was also shown to be correlated with nucleoids, the mitochondrial substructures involved in mtDNA processing. We observed different levels of colocalization between FISH and nucleoid markers, in agreement with the different amounts of regulatory proteins found in nucleoids and which might have regulatory functions (Chen and Butow, 2005; Shutt et al., 2011; Spelbrink, 2010).

mTRIP detects mitochondria and mitochondrial substructures rich in a given transcript. In addition to processed transcripts, mTRIP also appears to detect polycistronic RNAs, including signals compatible with transcripts of the complete H-strand, as well as RNA bound to the DNA template, the latter likely resulting from ongoing transcription. In general, we found a good correlation between RNA levels detected with mTRIP and RT-qPCR, thus validating the FISH approach described here which then allows assessing mitochondrial transcripts within the mitochondrial network, and in individual cells.

Labelling of DNA by mTRIP appears limited to locally open structures, as in transcription complexes after disruption of the RNA moiety, as well as in the transcription bubble at promoters, and in DNA engaged in initiation of replication. To date, identification of mitochondrial initiation of replication in single cells has been elusive. Importantly, mTRIP identifies a unique DNA region, targeted by mREP, that is distinct from but associated with the principal origin of replication O_H in humans. mTRIP also recognizes regions containing accessible DNA at the level of the O_L origin as well as a third mitochondrial replication origin expected to be activated only occasionally (Brown et al., 2005).

Importantly, at least three classes of mitochondrial structures are detected: (i) replication initiation active and transcript-positive (Ia-Tp), (ii) replication initiation silent and transcript-positive (Is-Tp), and (iii) replication initiation silent and transcript-negative (Is-Tn). The presence of these distinct structures reveals a large heterogeneity of mitochondria in single cells. In proliferating HeLa cells, Ia-Tp represent less than 15%, Is-Tp more than one half, and Is-Tn about one third of detected mitochondrial structures. mTRIP analysis may help in elucidating the link between mitochondrial DNA (i.e. ratio of Ia-Tp versus Is-Tp, and versus Is-Tn) and mitochondrial function. Moreover, the proportion of mitochondrial structures engaged in specific mtDNA processing activities appear dynamic, as they vary under stress and certain physiological conditions (Chatre and Ricchetti, 2013) and they may represent a significant parameter to take into account when assessing mitochondrial function.

Our data also highlight the heterogeneity of nucleic acids present at regulatory loci in the D-loop. In this context, mTRIP analysis identified DNA, RNA and RNA/DNA hybrids at the expected locations according to current knowledge on global mitochondrial populations (Chang and Clayton, 1985; Clayton, 1991; Falkenberg et al., 2007; Scarpulla, 2008), thus further validating this approach, which however operates in single cells. Indeed colocalization between probes pairs revealed accessible DNA, upstream of, and within the replication origin as well as at the level of promoter P_L on one side, and of promoters P_{H1} and P_{H2} on the other side. Accessible DNA appears the exclusive

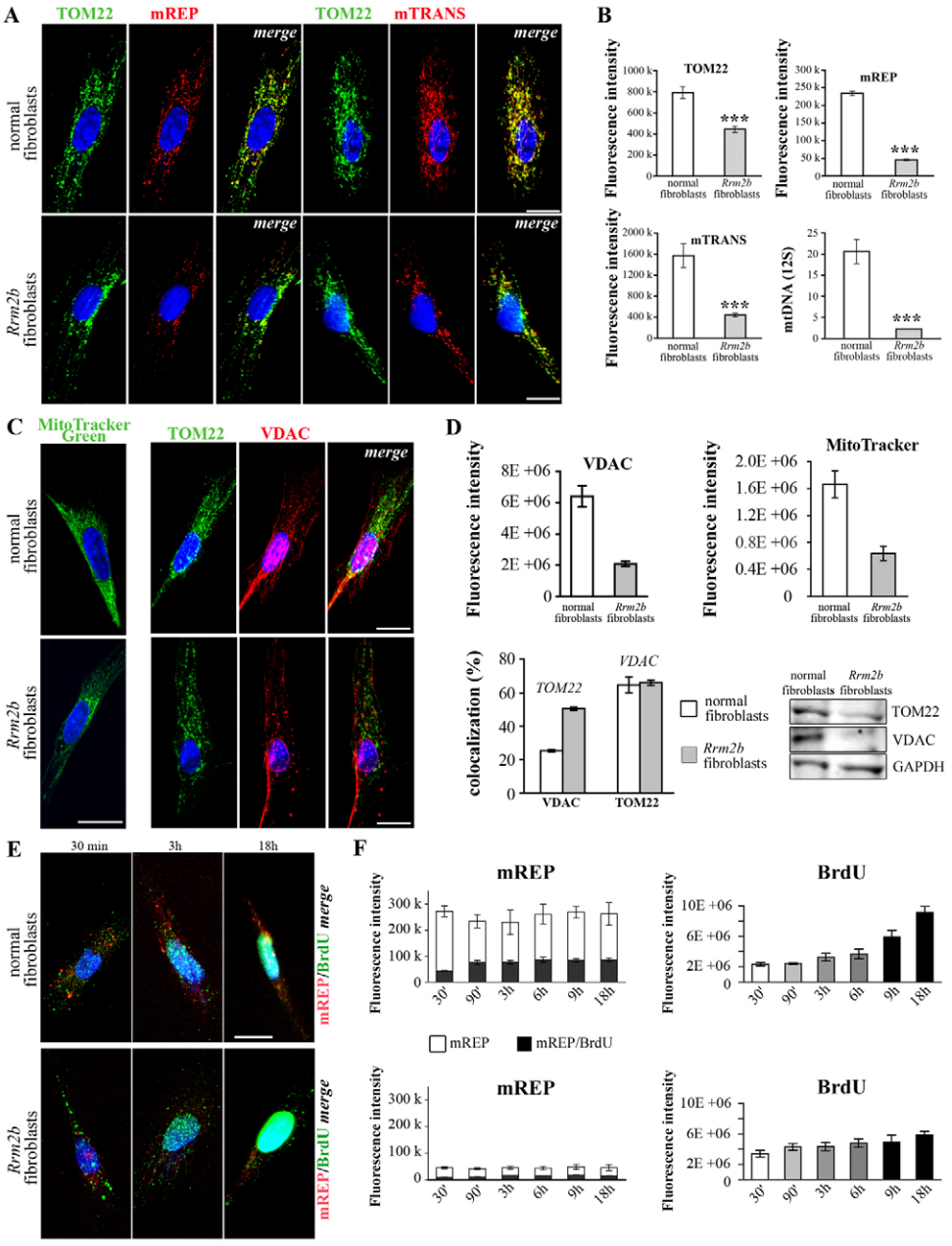

Fig. 7. mTRIP detects mtDNA processing alterations in cells of a patient with mitochondrial disease. (**A**) 3D-reconstructed normal human primary fibroblasts (IMR-90) and fibroblasts from a patient with mutated *Rrm2b* analysed by mTRIP with the probes mREP and mTRANS, co-labelled with TOM22 immunomarker. Single-labelling and merged images are shown. Results similar to IMR-90 were obtained with two other types of human primary fibroblasts (not shown). (**B**) Fluorescence intensity quantifications, and quantification of the mtDNA content (12S region) by qPCR. (**C**) The mitochondrial network of normal and *Rrm2b* fibroblasts is labelled with MitoTracker® Green. The mitochondrial mass is assessed with TOM22 (green), and with VDAC1/2/3 (red) co-immunolabelling. Note the different distribution of these two markers. (**D**) Fluorescence intensity quantification of markers in C, and colocalization of TOM22 and VDAC (the marker on the *x*-axis against the marker above the column). Bottom right-hand panel, western blot of TOM22 and VDAC in normal and mutant fibroblasts. (**E**) mREP and anti-BrdU co-labelling of normal and *Rrm2b* fibroblasts at the indicated time of exposure to BrdU. (**F**) Fluorescence intensity quantification (left-hand panels) of mREP (white) and mREP+/BrdU+ (black), and (right-hand panels) of BrdU (which cumulates nuclear and mitochondrial labelling). Note that, differently from HeLa cells, fibroblasts maintain constant colocalization levels of mREP/BrdU even after 18 h exposure to BrdU, suggesting that in these cells a large fraction of the replication bubble remains unproductive. Scale bars: 10 µm.

target upstream of O_H (from the mREP region to $PH_{1–2}$). Conversely, RNA is the almost exclusive target in the 16S region, as expected for P_{H1} transcripts, and a major target in the 7S region where it probably consists of L-strand transcripts. RNA/DNA hybrids are detected at P_L promoter compatibly with the formation of R-loops that provide the RNA primers for DNA replication, and also at a minor extent at 7S where they may represent L-transcripts bound to the DNA template. Importantly, the extent of colocalization among probes reveals comparable levels of labelling for the region mREP, that signals initiation of mtDNA replication, and the region that includes the O_H replication origin as well as the downstream 7S transcript. This observation is in agreement with the notion that L-strand transcription and replication are coupled (Scarpulla, 2008). Our data suggest that these two processes are not only temporally but also quantitatively linked.

In addition to these observations, our experiments provide novel information on the dynamics of some key regulatory regions of the mtDNA. In this context, accessible DNA in mREP, which is associated with O_H replication and L-strand transcription, appears also linked to H-strand transcription (for rRNAs) since about one half of mREP and PH1–2 signals colocalize. Importantly, however, lack of colocalization between the two probes indicates that in the other half of cases rRNA transcription is uncoupled to O_H replication. This result also underscores the region labelled by mREP, which is located close to key regulatory elements (P_L, $P_{H1–2}$, O_H) but does not contain significant regulatory elements itself. mREP nevertheless appears as a region whose accessibility acts as indicator of the dynamics of mtDNA replication and transcription of both the H- and the L-strand.

Moreover, transcription of the L-strand appears different in labelling from transcription of the H-strand (16S rRNA) in their

respective promoter regions since RNA/DNA hybrids, DNA, and RNA are detected in the former, and essentially RNA in the latter. Such difference could be associated with the lower transcription rate of the L-strand compared with rRNAs, or with the presence of structures linked to O_H replication. It is also possible that RNA/DNA hybrids and/or single-strand RNAs are functional to the transitory 7S triple strand structure, or else that 7S RNA labelled here has links with the specific RNA detected in immortalized cells (Duncan et al., 2000). A further difference between the two strands is the almost exclusive detection of accessible DNA at promoter P_{H1} whereas RNA/DNA hybrids are prevalently present at promoter P_L. Since the open DNA structure at P_H promoters is detected in the large majority of mitochondria, and this is also the case for the P_{H1} transcript 16S rRNA, transcription of rRNA provides the most abundant source of accessible DNA in the mitochondrial genome, at least detected by FISH.

Notably, only a limited fraction of mitochondria are recognized by probes that target the D-loop regulatory region (with the exception of $P_{H1–2}$ promoters). Non-labelled mitochondria either do not carry accessible DNA and/or RNA/DNA hybrids and/or L-transcripts in the respective regions, or the levels of these nucleic acids are below the threshold of detection. In both cases mTRIP reveals broad mitochondrial heterogeneity for the nucleic acid composition of the regulatory region of the mtDNA, which might have regulatory function.

In summary, by mTRIP the dynamics of mtDNA transcription and initiation of replication are exposed with unprecedented resolution at the single-cell level, and further classes are revealed when the D-loop regulatory region is dissected. Thus, mTRIP analysis may help in elucidating the link between mitochondrial DNA and the energizing state of individual cells, in particular in the context of diseases, and this approach may be used for future investigations of mtDNA processing under physiological and pathological conditions.

In this context, we also examined cells depleted in mtDNA, as is the case for several diseases (Rötig and Poulton, 2009), for example, *Rrm2b* fibroblasts, carrying a mutation that is associated with an mtDNA depletion syndrome (Bourdon et al., 2007). Here, reduced mtDNA transcription and replication were observed using mTRIP. In addition, we noted dramatically increased mitochondrial transcription and replication signals in cells with depleted mtDNA content following treatment with EtBr. This situation is compatible with the normal amounts of mitochondrial transcripts observed in HeLa cells depleted of mtDNA by EtBr treatment (Seidel-Rogol and Shadel, 2002). Moreover, it is likely also representative of muscle from patients with a particularly severe mtDNA depletion, which nevertheless displayed steady-state levels of mitochondrial transcription and had a surprisingly slow progression of the disease compared with other mtDNA depletion syndromes (Barthélémy et al., 2001). Thus, mTRIP reveals qualitative and quantitative alterations, which provide additional tools for elucidating mitochondrial dysfunction in diseases.

Materials and Methods

Cells and culture conditions

Human HeLa and HeLa *rho*^{0} cells, IMR90 fibroblasts (purchased from ATCC), and *Rrm2b* fibroblasts were grown in MEM medium with 10% foetal bovine serum (FBS) at 37℃ and in the presence of 5% CO_2. HeLa *rho*^{0} cells and *Rrm2b* fibroblasts were a kind gift from Dr Agnes Rötig (Genetics of mitochondrial disorders, Hôpital Necker, Paris). Cells under low oxidative stress were treated with 50 μM H_2O_2 for the time indicated. For mtDNA depletion, HeLa cells were treated with 25 μM EtBr for 3 days (King and Attardi, 1996).

Immunofluorescence, reagents and antibodies

Cells plated on slides were fixed with 2% PFA and permeabilized with 0.5% Triton X-100. The slides were incubated in blocking buffer (BSA 5% in PBS) for 1 h then with the primary antibody for 1 h. DNA was stained with 10 μg/ml Hoechst and the image analysis was carried out using Perkin-Elmer Ultraview RS Nipkow-spinning disk confocal microscope. BrdU, anti-TOM22 Atto488, Hoechst 33342, and ethidium bromide were purchased from Sigma; anti-BrdU antibody from BD Biosciences; MitoTracker® Green FM from Invitrogen, PCNA, TFAM, VDAC 1/2/3 (sc-98708), GADPH, and Polγ antibodies were purchased from Santa Cruz Biotechnology; goat anti-mouse and goat anti-rabbit Alexa® Fluor 488, Alexa® Fluor 555, and Cy5 conjugated secondary antibodies from Invitrogen.

Probe labelling and denaturation

DNA probes for FISH were labelled by nick translation of PCR products, incorporating Atto425-dUTP, or Atto488-dUTP, or Atto550-dUTP (Atto425/Atto488/Atto550 NT Labeling kit, Jena Bioscience). Forward and reverse primers for PCR amplification of DNA probes initiate at the position 'start' and 'end', respectively, in Table 1. Forty ng of labelled probes were mixed with 400 ng of sonicated salmon sperm DNA (Sigma) in hybridization buffer (50% formamide, 10% dextran sulfate, in 2×SSC pH 7.0), denatured at 80℃ for 10 min and kept at 37℃ for 30 min.

mTRIP and mTRIP-coupled immunofluorescence

Cells plated on slides were fixed with 2% PFA and permeabilized with 0.5% Triton X-100. Cells were then incubated in 50% formamide (pH=7.0)/2×SSC for 30 min at RT, and denatured in 70% formamide/2×SSC for 4 min at 75℃. Hybridization was performed with 40 ng of probe (single probe or mix) for 16 hrs at 37℃. After washing the slides in SSC, the DNA was stained with 10 μg/ml Hoechst. When required, fixed/permeabilized cells on slides were treated with RNaseA (100 μg/ml, Roche), or RNaseH (100 U/ml, NEB) or DNaseI (100 U/ml, Invitrogen) for 1 hr at 37℃, or with proteinase K (5 μg/ml, NEB) for 5 min at 37℃. When more than one nuclease were used, the enzymes were either added simultaneously or the second nuclease was added after incubation with the first nuclease, followed by three washes with PBS, and further incubation for 1 hr at 37℃. For mTRIP-coupled immunofluorescence, after hybridization and SSC wash, the immunofluorescence procedure (see above) was applied. The nuclease concentration for these experiments was tested with a dose-response test on several FISH probes (not shown).

Confocal acquisition, 3D-reconstruction and quantification

Confocal acquisitions were performed using a spinning-disk Perkin-Elmer Ultraview RS Nipkow Disk, an inverted laser-scanning confocal microscope Zeiss Axiovert 200 M with an Apochromat 63×/1.4 NA oil objective and a Hamamatsu ORCA II ER camera (Imagopole, PFID, Institut Pasteur). Images were acquired using non-saturating settings, and the same imaging parameters were used for all samples. Optical z-slices in 200-nm steps covering the whole depth of the cell were collected, at resolution of 1.024/1.024 pixels. Three-dimensional reconstruction of all the z-stacks was achieved using the 3D-volume rendering of IMARIS software (Bitplane). Original 2D images generated from 3D volume rendering were used for fluorescence quantification using the Integrated Density measurement tool of ImageJ 1.38×software (post-acquisition analysis). Graphic settings were applied to 2D images for the purpose of visualization (panels in figures). For each condition, 30 cells were analysed from three independent experiments. In certain co-labelling experiments with mREP (or mTRANS) and immunofluorescent markers, measurement of fluorescence of POLγ, TFAM or BrdU was performed in mREP-positive and mREP-negative (or in mTRANS-positive and in mTRANS-negative) areas, defined by identical circles and either containing or not the FISH marker. For each condition, 300 samples of identical surface, from at least 30 cells in three independent experiments, were analysed. Intensity correlation coefficient-based (ICCB) tools use global statistic analysis of pixel intensity distributions for colocalization analysis. The ImageJ plug-in JACoP is a compilation of the most relevant ICCB tools (e.g. Pearson's, Mander's and Costes's coefficients), and allows comparison of the various methods among them (Bolte and Cordelières, 2006). Colocalization studies were performed with ImageJ JACoP plug-in. Scale bars represent 10 μm, unless otherwise indicated.

Statistical analysis

The significance of differences between data was determined using Student's *t*-test for unpaired observations. *$P \leq 0.05$; **$P \leq 0.01$; ***$P \leq 0.001$.

RT-qPCR

Total RNA was isolated from HeLa cells using the RNeasy Mini kit (Qiagen), treated with DNaseI (Qiagen), then reverse-transcribed using Superscript®III Reverse transcriptase (Invitrogen). Real-time quantitative PCR was performed using Power SYBR Green PCR Master Mix (Applied Biosystems) and the rate of dye incorporation was monitored using the StepOne™ Plus RealTime PCR system (Applied Biosystems). Three biological replicates were used for each condition.

Data were analyzed by StepOne Plus RT PCR software v. 2.1 and Microsoft Excel. TBP transcript levels were used for normalisation of each target (=ΔCT). Real-time PCR C_T values were analyzed using the $2^{-\Delta\Delta Ct}$ method to calculate the fold expression (Schmittgen and Livak, 2008). Custom primers were designed using the Primer3Plus online software (http://www.bioinformatics.nl/cgi-bin/primer3plus/primer3plus.cgi). Primers used for amplifications are listed in supplementary material Table S1, with the corresponding references.

mtDNA content analysis by qPCR

The quantification of mtDNA was performed as described (Parone et al., 2008). Real-time PCR amplification was performed on 200 pg of total DNA using the StepOne™ Plus RealTime PCR system (Applied Biosystems) and Power SYBR Green PCR Master mix (ABI) following the manufacturer's instructions. Human mitochondrial DNA accession number NC012920 at [http://www.mitomap.org/bin/view.pl/MITOMAP/MitoSeqs]. The region tested on mtDNA was included in the 12S gene. The nuclear encoded 18S rRNA gene was used as an endogenous reference. The level of mtDNA was calculated using the ΔC_T of average C_T of mtDNA and nDNA ($\Delta C_T = C_T$ nDNA $- C_T$ mtDNA) as $2^{\Delta CT}$ (Fan et al., 2009). Primers used for amplification are listed in supplementary material Table S1.

Acknowledgements

We thank A. Rötig for the kind gift of HeLa *rho*^{0} cells and *Rrm2b* fibroblasts. We also thank L. Arbibe and collaborators for helpful discussion, F. Brandizzi, B. Dujon, S. Tajbakhsh and C. Zurzolo, for comments on the manuscript, and the Imagopole (PFID) of Institut Pasteur for advice. The mTRIP protocol is the subject of the International patent application number PCT/EP2012/054739.

Funding

This work was supported by the ARC (Association Nationale contre le Cancer); and PTR-Institut Pasteur. L.C. was the recipient of a Bourse Roux and was supported by F. Lacoste.

Supplementary material available online at
http://jcs.biologists.org/lookup/suppl/doi:10.1242/jcs.114322/-/DC1

References

Acquaviva, F., De Biase, I., Nezi, L., Ruggiero, G., Tatangelo, F., Pisano, C., Monticelli, A., Garbi, C., Acquaviva, A. M. and Cocozza, S. (2005). Extra-mitochondrial localisation of frataxin and its association with IscU1 during enterocyte-like differentiation of the human colon adenocarcinoma cell line Caco-2. *J. Cell Sci.* **118**, 3917-3924.

Alán, L., Zelenka, J., Ježek, J., Dlasková, A. and Ježek, P. (2010). Fluorescent in situ hybridization of mitochondrial DNA and RNA. *Acta Biochim. Pol.* **57**, 403-408.

Antes, A., Tappin, I., Chung, S., Lim, R., Lu, B., Parrott, A. M., Hill, H. Z., Suzuki, C. K. and Lee, C. G. (2010). Differential regulation of full-length genome and a single-stranded 7S DNA along the cell cycle in human mitochondria. *Nucleic Acids Res.* **38**, 6466-6476.

Arabi, A., Wu, S., Ridderstråle, K., Bierhoff, H., Shiue, C., Fatyol, K., Fahlén, S., Hydbring, P., Söderberg, O., Grummt, I. et al. (2005). c-Myc associates with ribosomal DNA and activates RNA polymerase I transcription. *Nat. Cell Biol.* **7**, 303-310.

Barthélémy, C., Ogier de Baulny, H., Diaz, J., Cheval, M. A., Frachon, P., Romero, N., Goutieres, F., Fardeau, M. and Lombès, A. (2001). Late-onset mitochondrial DNA depletion: DNA copy number, multiple deletions, and compensation. *Ann. Neurol.* **49**, 607-617.

Bolte, S. and Cordelières, F. P. (2006). A guided tour into subcellular colocalization analysis in light microscopy. *J. Microsc.* **224**, 213-232.

Bonawitz, N. D., Clayton, D. A. and Shadel, G. S. (2006). Initiation and beyond: multiple functions of the human mitochondrial transcription machinery. *Mol. Cell* **24**, 813-825.

Bourdon, A., Minai, L., Serre, V., Jais, J. P., Sarzi, E., Aubert, S., Chrétien, D., de Lonlay, P., Paquis-Flucklinger, V., Arakawa, H. et al. (2007). Mutation of RRM2B, encoding p53-controlled ribonucleotide reductase (p53R2), causes severe mitochondrial DNA depletion. *Nat. Genet.* **39**, 776-780.

Brown, T. A., Cecconi, C., Tkachuk, A. N., Bustamante, C. and Clayton, D. A. (2005). Replication of mitochondrial DNA occurs by strand displacement with alternative light-strand origins, not via a strand-coupled mechanism. *Genes Dev.* **19**, 2466-2476.

Brown, T. A., Tkachuk, A. N. and Clayton, D. A. (2008). Native R-loops persist throughout the mouse mitochondrial DNA genome. *J. Biol. Chem.* **283**, 36743-36751.

Brown, T. A., Tkachuk, A. N., Shtengel, G., Kopek, B. G., Bogenhagen, D. F., Hess, H. F. and Clayton, D. A. (2011). Superresolution fluorescence imaging of mitochondrial nucleoids reveals their spatial range, limits, and membrane interaction. *Mol. Cell. Biol.* **31**, 4994-5010.

Chan, D. C. (2006). Mitochondrial fusion and fission in mammals. *Annu. Rev. Cell Dev. Biol.* **22**, 79-99.

Chang, D. D. and Clayton, D. A. (1985). Priming of human mitochondrial DNA replication occurs at the light-strand promoter. *Proc. Natl. Acad. Sci. USA* **82**, 351-355.

Chatre, L. and Ricchetti, M. (2013). Prevalent coordination of mitochondrial DNA transcription and initiation of replication with the cell cycle. *Nucl. Acids Res.* **41**, 3068-3078.

Chen, X. J. and Butow, R. A. (2005). The organization and inheritance of the mitochondrial genome. *Nat. Rev. Genet.* **6**, 815-825.

Clayton, D. A. (1991). Replication and transcription of vertebrate mitochondrial DNA. *Annu. Rev. Cell Biol.* **7**, 453-478.

Davis, A. F. and Clayton, D. A. (1996). In situ localization of mitochondrial DNA replication in intact mammalian cells. *J. Cell Biol.* **135**, 883-893.

De Pinto, V., Messina, A., Lane, D. J. and Lawen, A. (2010). Voltage-dependent anion-selective channel (VDAC) in the plasma membrane. *FEBS Lett.* **584**, 1793-1799.

de Planell-Saguer, M., Rodicio, M. C. and Mourelatos, Z. (2010). Rapid in situ codetection of noncoding RNAs and proteins in cells and formalin-fixed paraffin-embedded tissue sections without protease treatment. *Nat. Protoc.* **5**, 1061-1073.

Duncan, E. L., Perrem, K. and Reddel, R. R. (2000). Identification of a novel human mitochondrial D-loop RNA species which exhibits upregulated expression following cellular immortalization. *Biochem. Biophys. Res. Commun.* **276**, 439-446.

Echave, P., Machado-da-Silva, G., Arkell, R. S., Duchen, M. R., Jacobson, J., Mitter, R. and Lloyd, A. C. (2009). Extracellular growth factors and mitogens cooperate to drive mitochondrial biogenesis. *J. Cell Sci.* **122**, 4516-4525.

Falkenberg, M., Larsson, N. G. and Gustafsson, C. M. (2007). DNA replication and transcription in mammalian mitochondria. *Annu. Rev. Biochem.* **76**, 679-699.

Fan, A. X., Radpour, R., Haghighi, M. M., Kohler, C., Xia, P., Hahn, S., Holzgreve, W. and Zhong, X. Y. (2009). Mitochondrial DNA content in paired normal and cancerous breast tissue samples from patients with breast cancer. *J. Cancer Res. Clin. Oncol.* **135**, 983-989.

Holt, I. J., Lorimer, H. E. and Jacobs, H. T. (2000). Coupled leading- and lagging-strand synthesis of mammalian mitochondrial DNA. *Cell* **100**, 515-524.

Isobe, K., Suda, A., Hashimoto, H., Kannari, F., Kawano, H., Mizuno, H., Miyawaki, A. and Midorikawa, K. (2010). High-resolution fluorescence microscopy based on a cyclic sequential multiphoton process. *Biomed. Opt. Express* **1**, 791-797.

King, M. P. and Attardi, G. (1996). Isolation of human cell lines lacking mitochondrial DNA. *Methods Enzymol.* **264**, 304-313.

Kukat, C., Wurm, C. A., Spåhr, H., Falkenberg, M., Larsson, N. G. and Jakobs, S. (2011). Super-resolution microscopy reveals that mammalian mitochondrial nucleoids have a uniform size and frequently contain a single copy of mtDNA. *Proc. Natl. Acad. Sci. USA* **108**, 13534-13539.

Latil, M., Rocheteau, P., Châtre, L., Sanulli, S., Mémet, S., Ricchetti, M., Tajbakhsh, S. and Chrétien, F. (2012). Skeletal muscle stem cells adopt a dormant cell state post mortem and retain regenerative capacity. *Nat. Commun.* **3**, 903.

Lee, S., Kim, S., Sun, X., Lee, J. H. and Cho, H. (2007). Cell cycle-dependent mitochondrial biogenesis and dynamics in mammalian cells. *Biochem. Biophys. Res. Commun.* **357**, 111-117.

Masny, P. S., Chan, O. Y., de Greef, J. C., Bengtsson, U., Ehrlich, M., Tawil, R., Lock, L. F., Hewitt, J. E., Stocksdale, J., Martin, J. H. et al. (2010). Analysis of allele-specific RNA transcription in FSHD by RNA-DNA FISH in single myonuclei. *Eur. J. Hum. Genet.* **18**, 448-456.

Mitra, K., Wunder, C., Roysam, B., Lin, G. and Lippincott-Schwartz, J. (2009). A hyperfused mitochondrial state achieved at G1-S regulates cyclin E buildup and entry into S phase. *Proc. Natl. Acad. Sci. USA* **106**, 11960-11965.

Ojala, D., Montoya, J. and Attardi, G. (1981). tRNA punctuation model of RNA processing in human mitochondria. *Nature* **290**, 470-474.

Ozawa, T., Natori, Y., Sato, M. and Umezawa, Y. (2007). Imaging dynamics of endogenous mitochondrial RNA in single living cells. *Nat. Methods* **4**, 413-419.

Parfait, B., Rustin, P., Munnich, A. and Rötig, A. (1998). Co-amplification of nuclear pseudogenes and assessment of heteroplasmy of mitochondrial DNA mutations. *Biochem. Biophys. Res. Commun.* **247**, 57-59.

Parone, P. A., Da Cruz, S., Tondera, D., Mattenberger, Y., James, D. I., Maechler, P., Barja, F. and Martinou, J. C. (2008). Preventing mitochondrial fission impairs mitochondrial function and leads to loss of mitochondrial DNA. *PLoS ONE* **3**, e3257.

Poulton, J., Morten, K., Freeman-Emmerson, C., Potter, C., Sewry, C., Dubowitz, V., Kidd, H., Stephenson, J., Whitehouse, W., Hansen, F. J. et al. (1994). Deficiency of the human mitochondrial transcription factor h-mtTFA in infantile mitochondrial myopathy is associated with mtDNA depletion. *Hum. Mol. Genet.* **3**, 1763-1769.

Rötig, A. and Poulton, J. (2009). Genetic causes of mitochondrial DNA depletion in humans. *Biochim. Biophys. Acta* **1792**, 1103-1108.

Scarpulla, R. C. (2008). Transcriptional paradigms in mammalian mitochondrial biogenesis and function. *Physiol. Rev.* **88**, 611-638.

Schmittgen, T. D. and Livak, K. J. (2008). Analyzing real-time PCR data by the comparative C(T) method. *Nat. Protoc.* **3**, 1101-1108.

Seidel-Rogol, B. L. and Shadel, G. S. (2002). Modulation of mitochondrial transcription in response to mtDNA depletion and repletion in HeLa cells. *Nucleic Acids Res.* **30**, 1929-1934.

Shutt, T. E., Lodeiro, M. F., Cotney, J., Cameron, C. E. and Shadel, G. S. (2010). Core human mitochondrial transcription apparatus is a regulated two-component system in vitro. *Proc. Natl. Acad. Sci. USA* **107**, 12133-12138.

Shutt, T. E., Bestwick, M. and Shadel, G. S. (2011). The core human mitochondrial transcription initiation complex: It only takes two to tango. *Transcription* **2**, 55-59.

Spelbrink, J. N. (2010). Functional organization of mammalian mitochondrial DNA in nucleoids: history, recent developments, and future challenges. *IUBMB Life* **62**, 19-32.

Yano, M., Hoogenraad, N., Terada, K. and Mori, M. (2000). Identification and functional analysis of human Tom22 for protein import into mitochondria. *Mol. Cell. Biol.* **20**, 7205-7213.

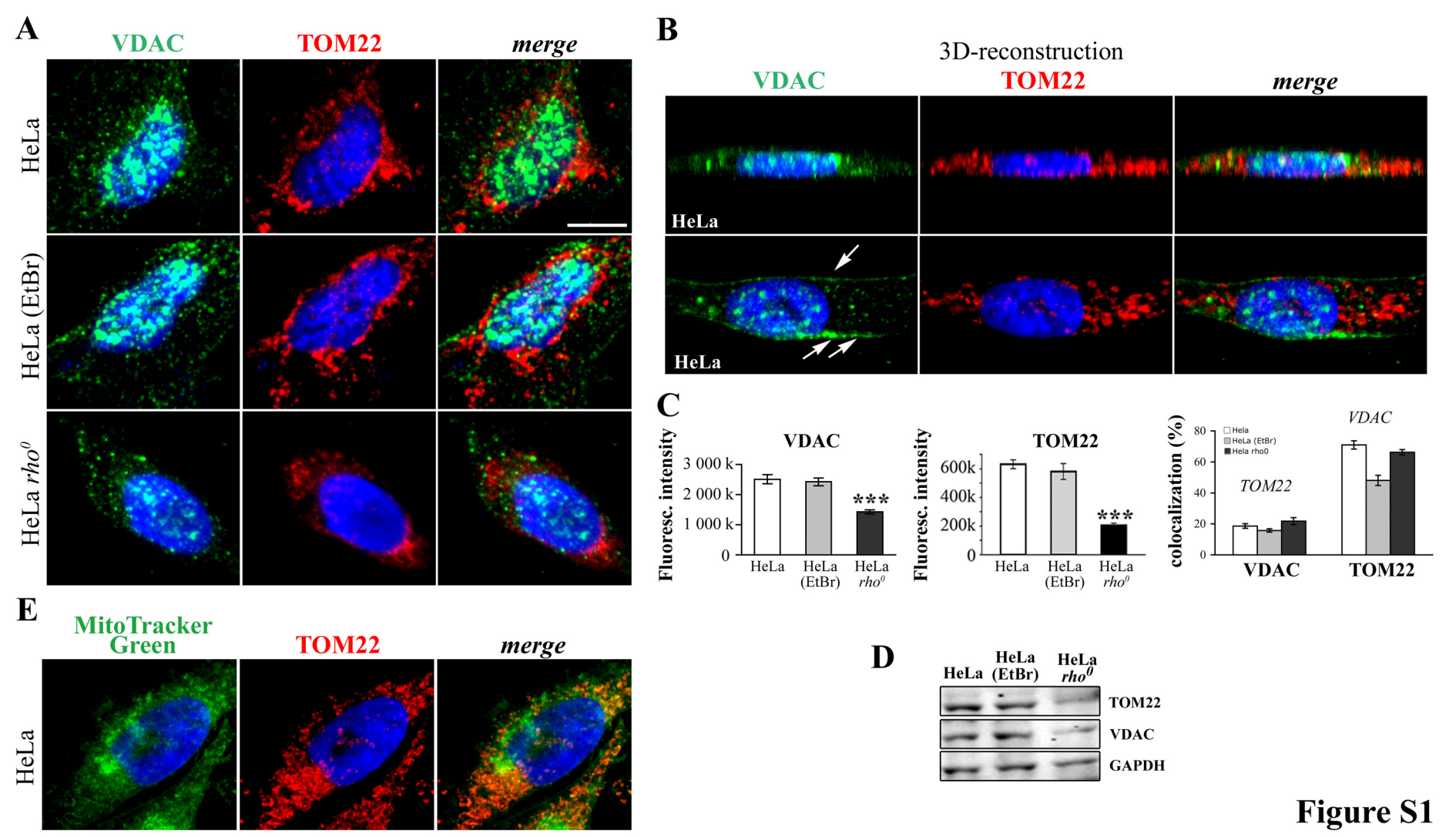
A
VDAC
TOM22
merge
HeLa
HeLa (EtBr)
HeLa rho0
B
3D-reconstruction
VDAC
TOM22
merge
HeLa
HeLa
C
VDAC
Fluoresc. intensity
3 000 k
2 000 k
1 000 k
0
***
HeLa
HeLa (EtBr)
HeLa rho0
TOM22
Fluoresc. intensity
600k
400k
200k
0
***
HeLa
HeLa (EtBr)
HeLa rho0
colocalization (%)
Hela
HeLa (EtBr)
Hela rho0
TOM22
VDAC
80
60
40
20
0
VDAC
TOM22
D
HeLa
HeLa (EtBr)
HeLa rho0
TOM22
VDAC
GAPDH
E
MitoTracker Green
TOM22
merge
HeLa

Figure S1

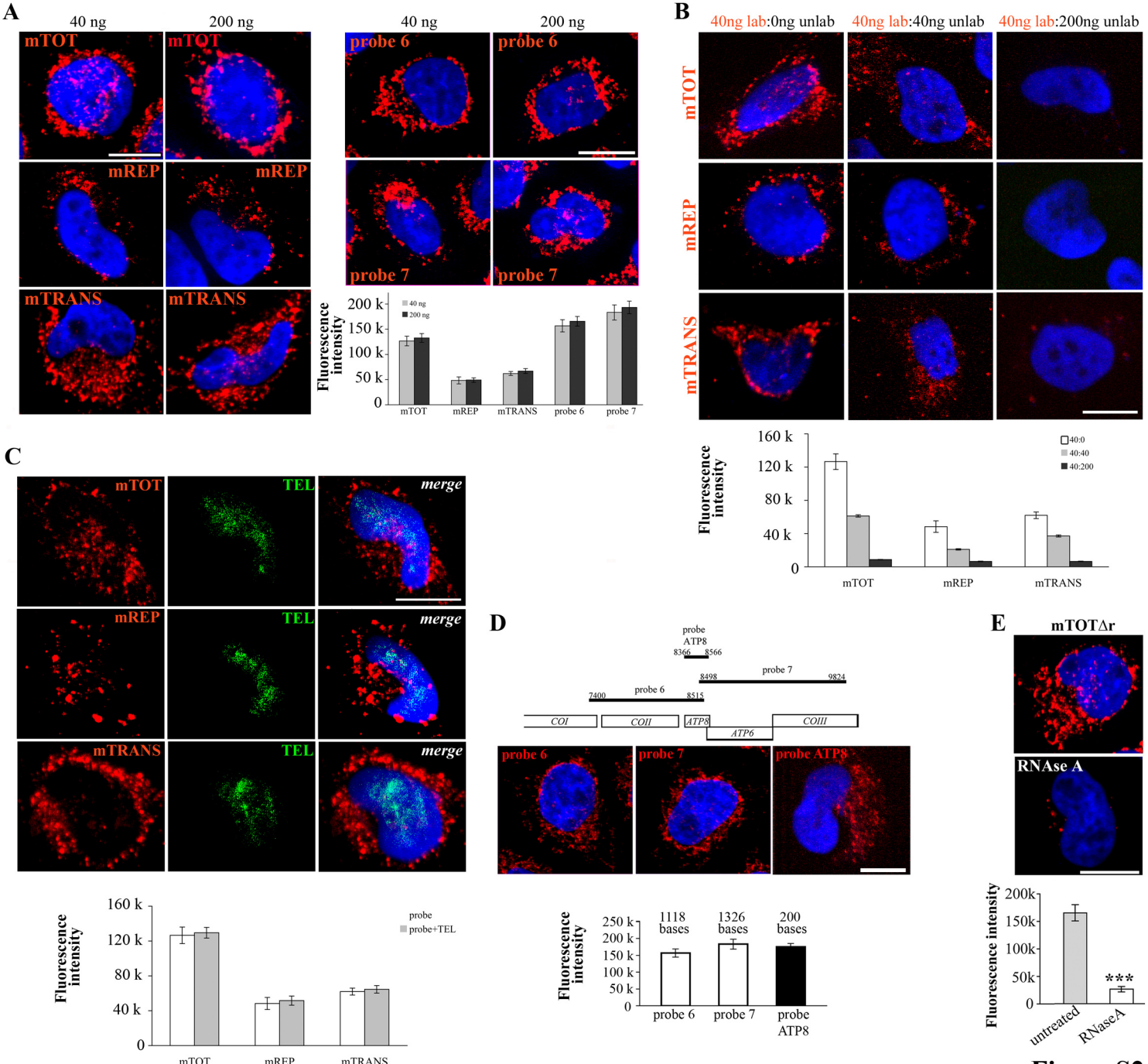
A
40 ng
200 ng
mTOT
mREP
mTRANS
probe 6
probe 7
Fluorescence intensity
200 k
150 k
100 k
50 k
0
40 ng
200 ng
mTOT
mREP
mTRANS
probe 6
probe 7
B
40ng lab:0ng unlab
40ng lab:40ng unlab
40ng lab:200ng unlab
mTOT
mREP
mTRANS
Fluorescence intensity
160 k
120 k
80 k
40 k
0
40:0
40:40
40:200
mTOT
mREP
mTRANS
C
mTOT
mREP
mTRANS
TEL
merge
Fluorescence intensity
160 k
120 k
80 k
40 k
0
probe
probe+TEL
mTOT
mREP
mTRANS
D
probe
ATP8
8366
8566
probe 7
8498
9824
probe 6
7400
8515
COI
COII
ATP8
ATP6
COIII
probe 6
probe 7
probe ATP8
Fluorescence intensity
250 k
200 k
150 k
100 k
50 k
0
1118 bases
1326 bases
200 bases
probe 6
probe 7
probe ATP8
E
mTOTΔr
RNAse A
Fluorescence intensity
200k
150k
100k
50k
0
***
untreated
RNaseA

Figure S2

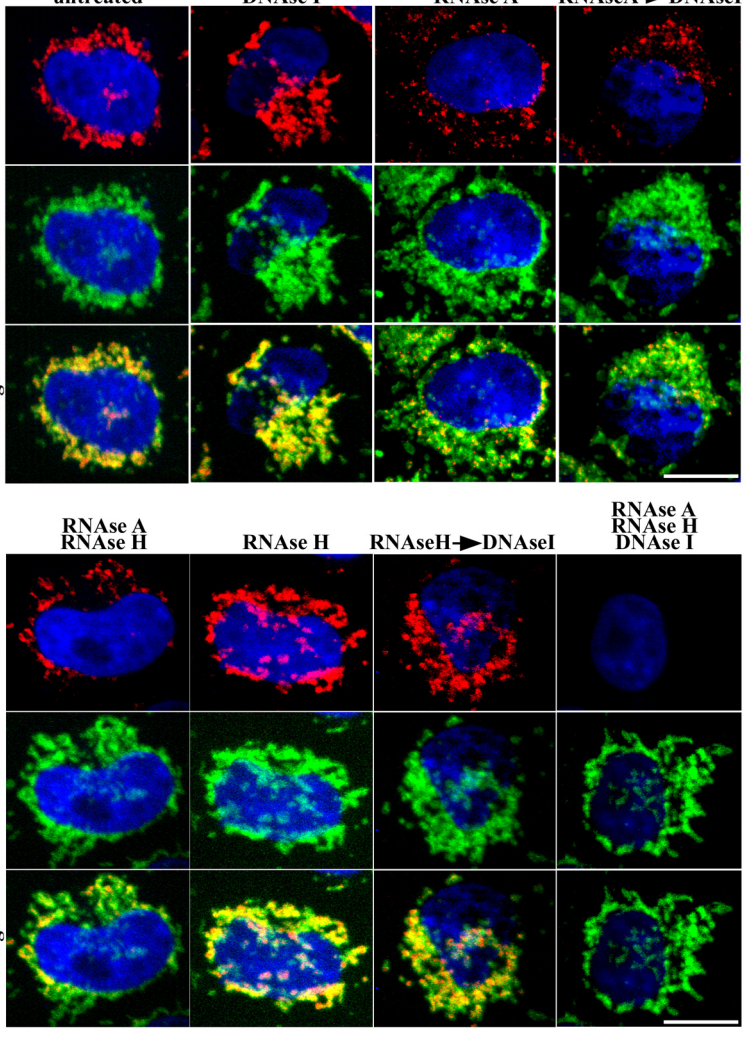
untreated
DNAse I
RNAse A
RNAseA➔DNAseI
mTOT
TOM22
merge
RNAse A
RNAse H
RNAse H
RNAseH➔DNAseI
RNAse A
RNAse H
DNAse I
mTOT
TOM22
merge

Figure S3

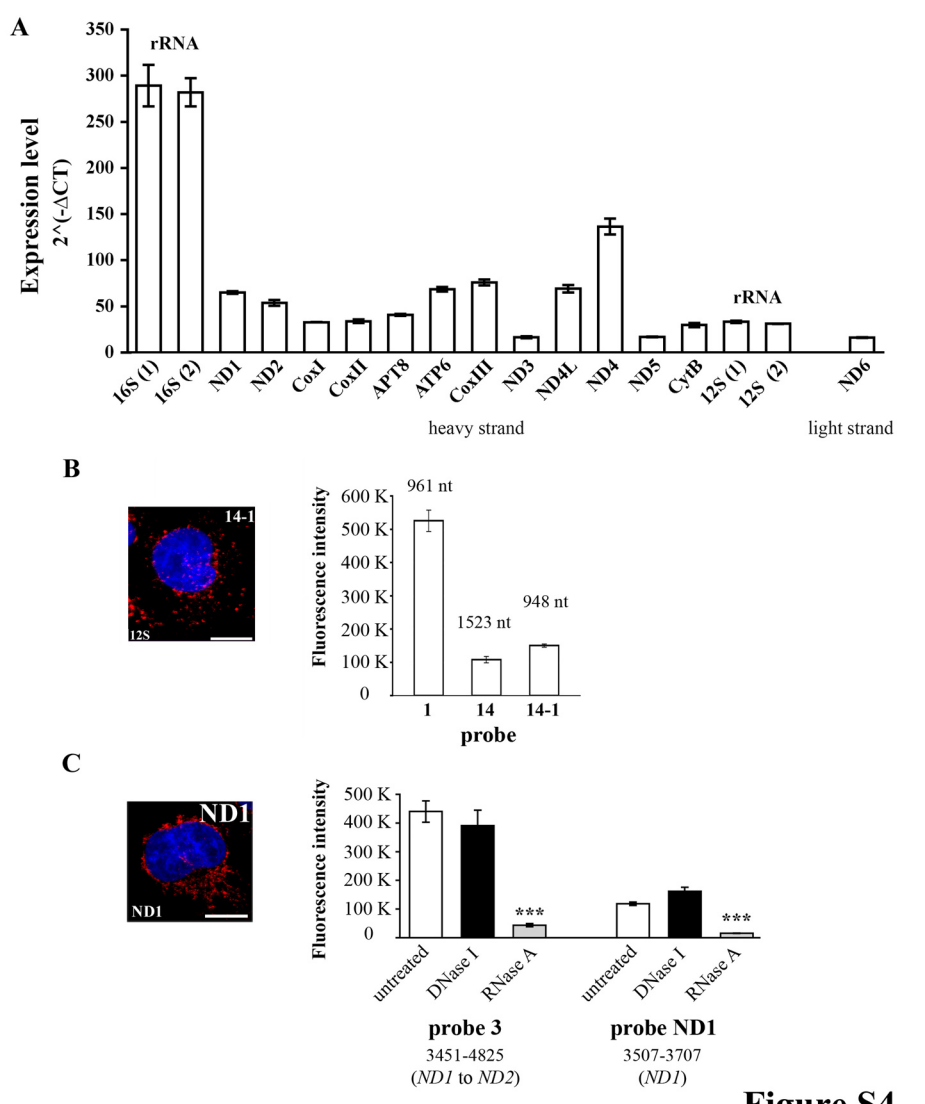
A
Expression level
2^(-ΔCT)
350
300
250
200
150
100
50
0
rRNA
rRNA
16S (1)
16S (2)
ND1
ND2
CoxI
CoxII
APT8
ATP6
CoxIII
ND3
ND4L
ND4
ND5
CytB
12S (1)
12S (2)
ND6
heavy strand
light strand
B
14-1
12S
961 nt
948 nt
1523 nt
Fluorescence intensity
600 K
500 K
400 K
300 K
200 K
100 K
0
1
14
14-1
probe
C
ND1
ND1
500 K
400 K
300 K
200 K
100 K
0
***
***
untreated
DNase I
RNase A
untreated
DNase I
RNase A
probe 3
3451-4825
(ND1 to ND2)
probe ND1
3507-3707
(ND1)

Figure S4

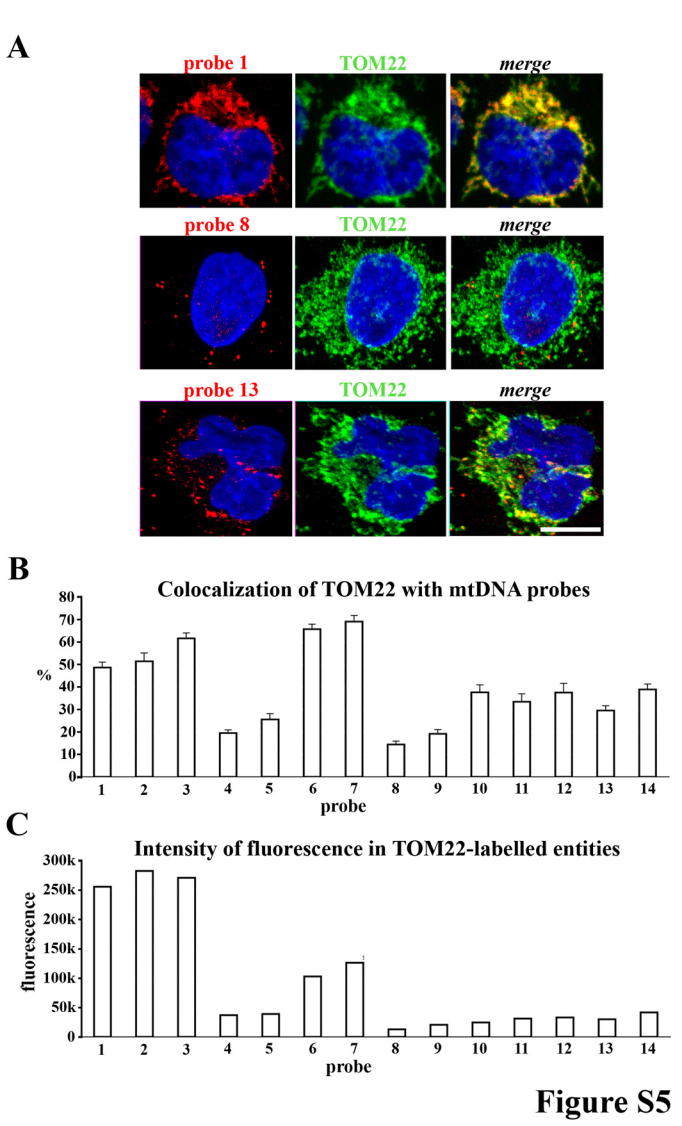
A
probe 1
TOM22
merge
probe 8
TOM22
merge
probe 13
TOM22
merge
B
Colocalization of TOM22 with mtDNA probes
%
80
70
60
50
40
30
20
10
0
1
2
3
4
5
6
7
8
9
10
11
12
13
14
probe
C
Intensity of fluorescence in TOM22-labelled entities
fluorescence
300k
250k
200k
150k
100k
50k
0
1
2
3
4
5
6
7
8
9
10
11
12
13
14
probe

Figure S5

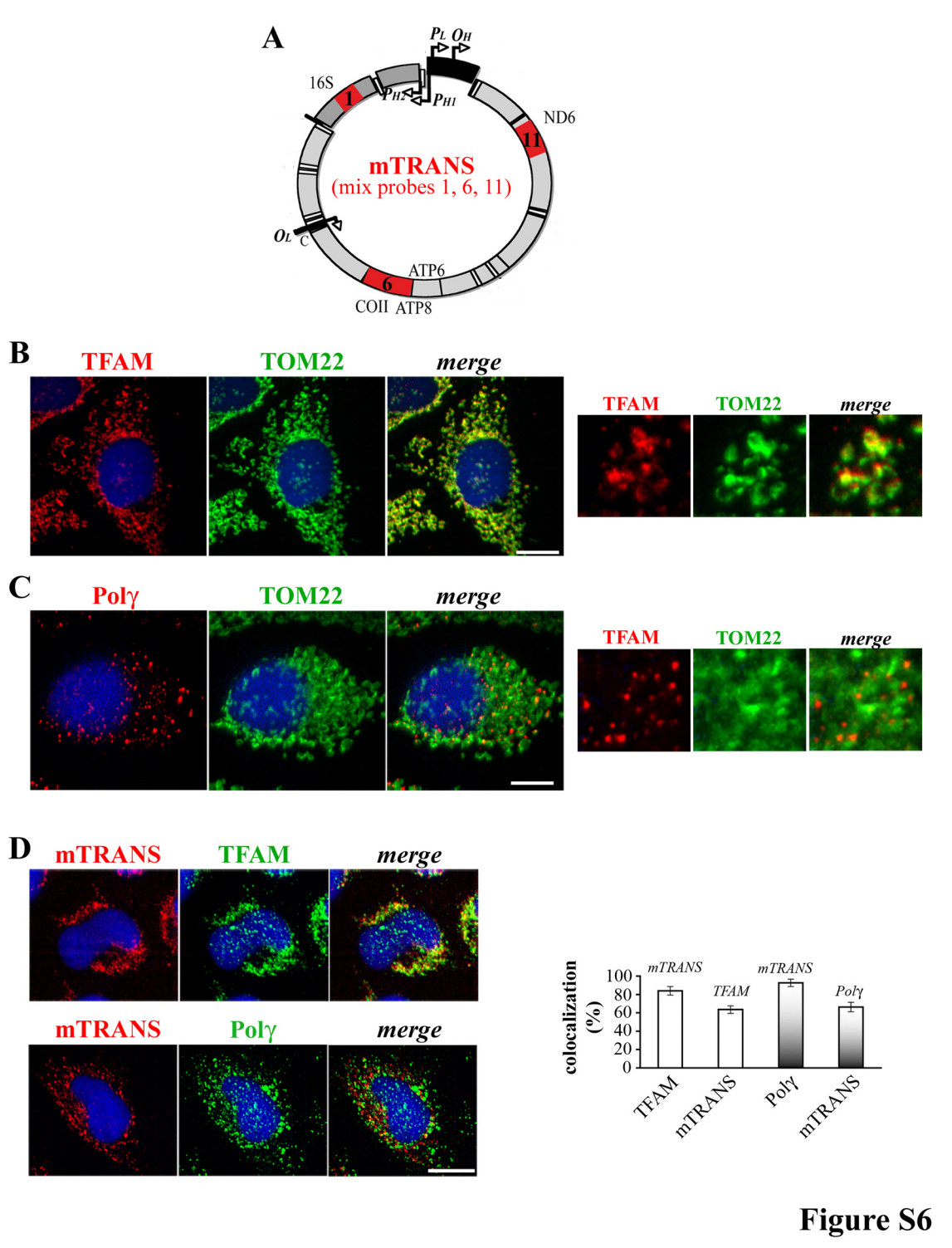
A
PL OH
16S
1
PH2
PH1
ND6
11
mTRANS
(mix probes 1, 6, 11)
OL
C
ATP6
6
COII ATP8
B
TFAM
TOM22
merge
TFAM
TOM22
merge
C
Polγ
TOM22
merge
TFAM
TOM22
merge
D
mTRANS
TFAM
merge
mTRANS
Polγ
merge
colocalization (%)
100
80
60
40
20
0
mTRANS
TFAM
mTRANS
Polγ
TFAM
mTRANS
Polγ
mTRANS

Figure S6

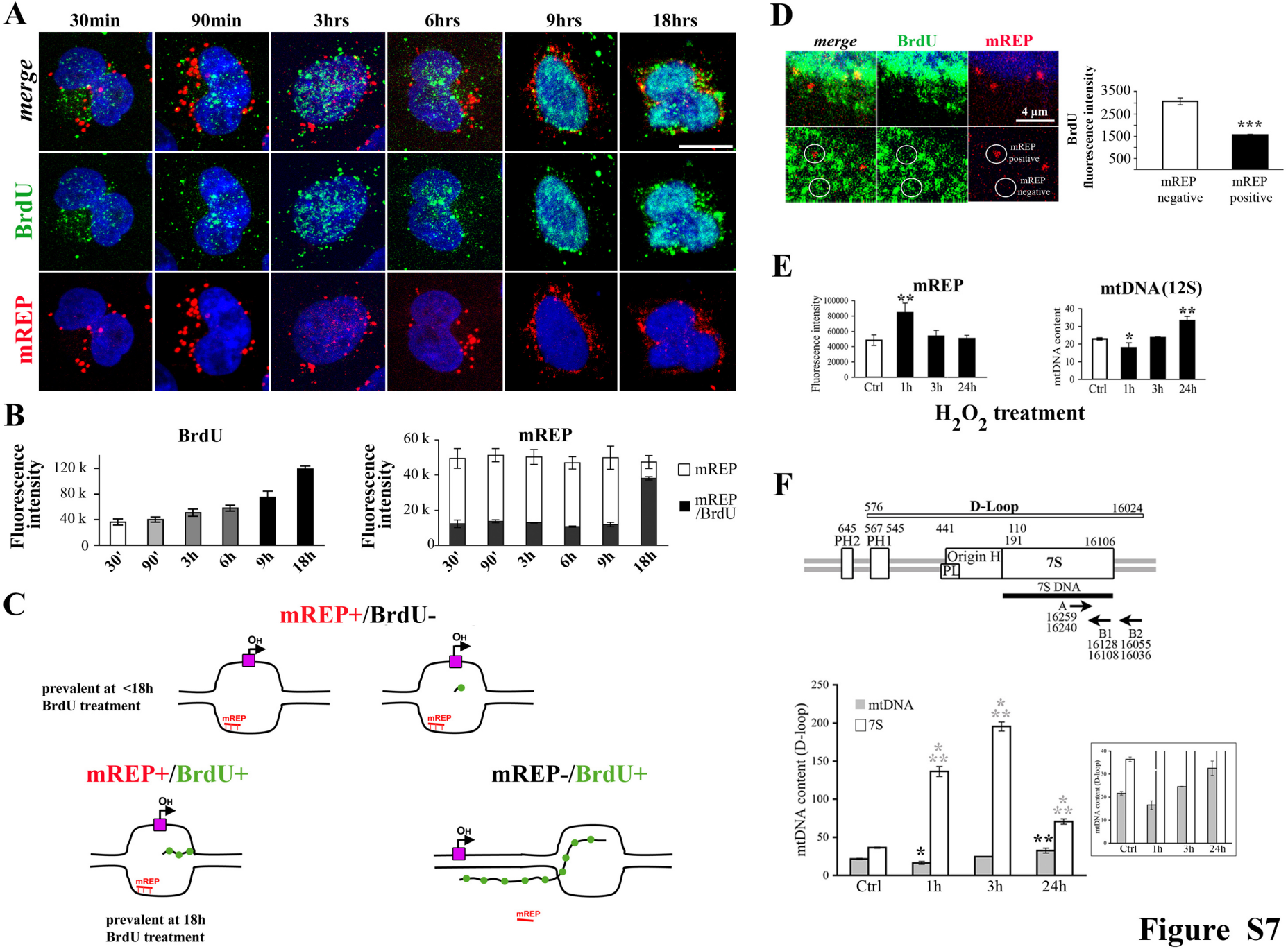
A
30min
90min
3hrs
6hrs
9hrs
18hrs
merge
BrdU
mREP
B
BrdU
Fluorescence intensity
120 k
80 k
40 k
0
30'
90'
3h
6h
9h
18h
mREP
60 k
40 k
20 k
0
mREP
/BrdU
C
mREP+/BrdU-
prevalent at <18h
BrdU treatment
OH
mREP
mREP+/BrdU+
mREP-/BrdU+
prevalent at 18h
BrdU treatment
D
merge
BrdU
mREP
4 μm
mREP positive
mREP negative
BrdU fluorescence intensity
3500
2500
1500
500
***
mREP negative
mREP positive
E
mREP
Fluorescence intensity
100000
80000
60000
40000
20000
0
**
Ctrl
1h
3h
24h
mtDNA (12S)
mtDNA content
40
30
20
10
0
*
**
H2O2 treatment
F
576
D-Loop
16024
645
PH2
567
PH1
545
441
110
191
16106
Origin H
PL
7S
7S DNA
A
16259
16240
B1
16128
16108
B2
16055
16036
mtDNA content (D-loop)
250
200
150
100
50
0
mtDNA
7S
*
**
Ctrl
1h
3h
24h

Figure S7

A

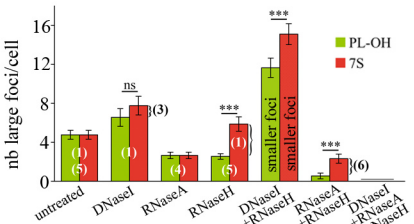

B

large foci

PL-OH	7S	
RNA/DNA	RNA	pattern (1)
-	DNA a/o RNA a/o RNA/DNA	pattern (2)
DNA	RNA a/o RNA/DNA	pattern (3)
RNA/DNA	DNA a/o RNA/DNA	pattern (4)
RNA (a/o RHR-RNA/DNA)	RNA (a/o RHR-RNA/DNA)	pattern (5)
-	DNA	pattern (6)

Figure S8

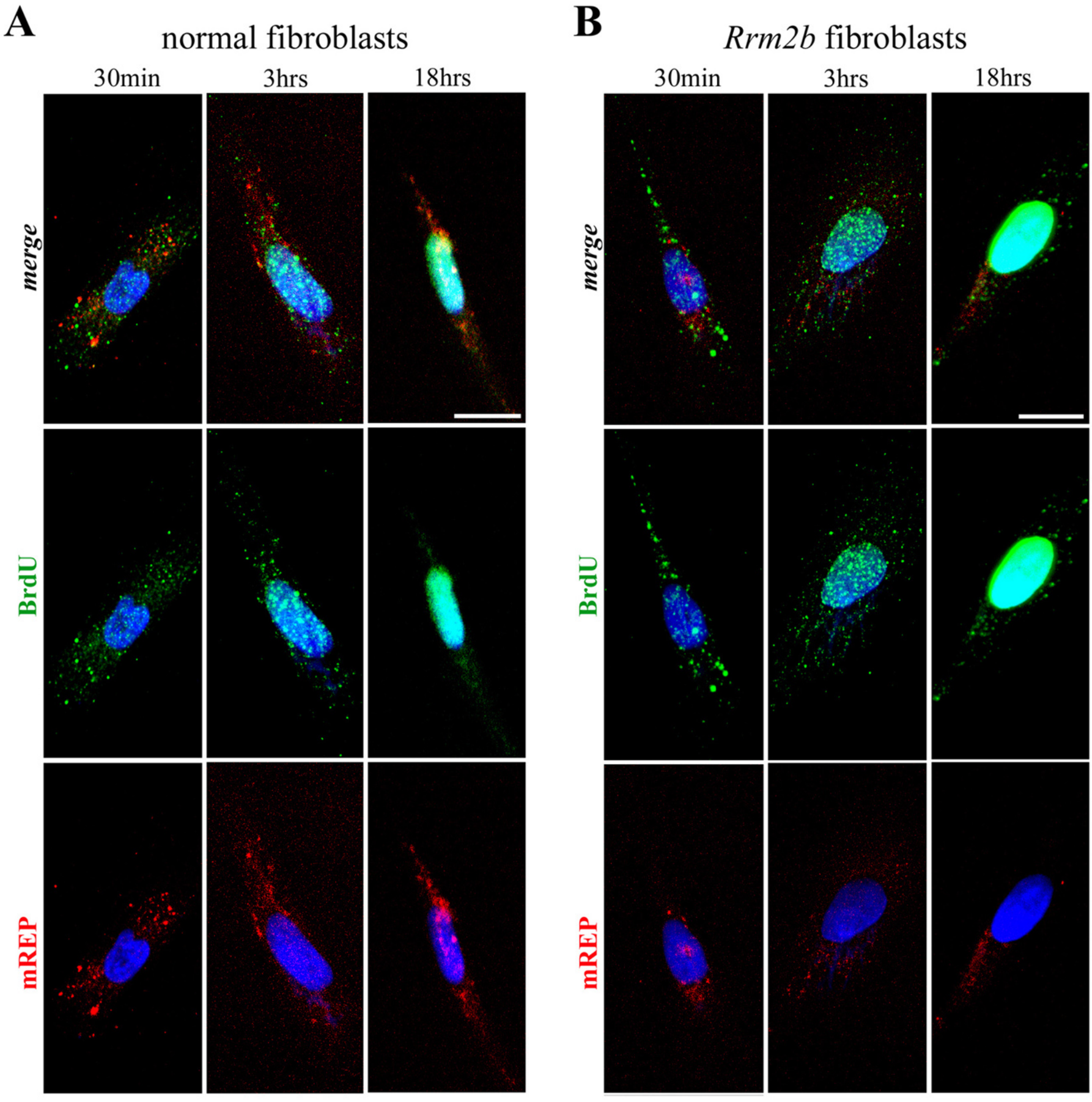
A
normal fibroblasts
30min
3hrs
18hrs
merge
BrdU
mREP
B
Rrm2b fibroblasts
30min
3hrs
18hrs
merge
BrdU
mREP

Figure S9

Supplementary Figure legends

Figure S1. Detection of the mitochondrial network in HeLa cells. (A) 3D-reconstructed HeLa cells (upper panels) immunolabeled with VDAC1/2/3 (green), TOM22 (red), and merge. Nuclei are labeleld with Hoechst (blue). Note the large VDAC (but not TOM22) signal in the correspondence of the nucleus, in agreement with several reports showing that VDACs are localized also in extramitochondrial membranes, including the plasma membrane and the endoplasmic reticulum, ER, (De Pinto et al., 2010, *FEBS Lett*. 584: 1793-1799; Mathupala and Pedersen, 2010, *Cancer Biol. Ther.* 9: 1053-1056; Elinder et al., 2005 *Cell Death Differ*. 12: 1134-1140; Shoshan-Barmatz and Israelson, 2005, *J. Membr. Biol*. 204:57-66; Bahamonde et al, 2003, *J. Biol. Chem.* 278: 33284-33289; Thinnes, 1992, *J. Bioenerg. Biomembr*. 24:71-75). The perninuclear labelling of VDAC in this panel is in agreement with its detected presence in the perinuclear ER. Different intracellular VDAC versus TOM22 labelling is also shown in HeLa cells treated for three days with EtBr to deplete the mtDNA (middle panels), and HeLa *rho*^{0} cells, which contain mitochondria but not mtDNA (lower panels). EtBr-treated Hela cells and *rho*^{0} cells are used later in this study. **(B)** Two plans of the 3D-volume rendering of a HeLa cell labelled as in panel (A). Note also the presence of VDAC (but not TOM22) at the extreme periphery of the cytoplasm (white arrows), likely in the plasma membrane. **(C)** Quantification of the fluorescence intensity of VDAC and of TOM22 (values of TOM22 are from Fig. 6B). The right panel shows colocalization of VDAC (on the X-axis) with TOM22, and of TOM22 (on the X-axis) with VDAC in untreated, EtBr-treated, and *rho*^{0} HeLa cells. A large fraction of VDAC does not colocalize with TOM22, compatibly with the localization of VDAC, but not of TOM22, in the nuclear region and in other extramitochondrial membranes (see above). Conversely, TOM22 largely colocalizes with VDAC. Note that the absence of colocalization may also be due to one of the two markers being present below the detection level. Moreover, the heterogeneity of intramitochondrial localization of VDAC versus TOM22 (VDAC1/2 are present in specific domains of the mitochondrial membrane, Neumann et al, 2010, *PMC Biophysics*, 3:4. TOM22 appears homogenously diffused in the mitochondria, Yano et al, 200, *Mol. Cell. Biol* 19: 7205-7213) may also be responsible for the absence of colocalization signal at certain positions. **(D)** Western blot of TOM22 and VDAC in untreated, EtBr-treated and *rho*^{0} HeLa cells show that each of the two proteins is present at comparable levels in untreated and EtBr-treated cells, whereas the levels drop in *rho*^{0} cells, in agreement with immunofluorescence data. **(E)** Colocalization of MitoTracker® Green FM, a green–fluorescent mitochondrial stain that selectively accumulates in the mitochondrial matrix, and TOM22. Scale bar = 10 μm.

Figure S2. mTRIP signal is specific and is not limited by probe concentration nor is affected by probe size. (A) 3D-reconstructed HeLa cells labeled with the mTOT probe (red) at saturating (200 ng) and at regular concentrations (40 ng), upper panels. Additional four probes used in this study (mREP, mTRANS, probes 6 and 7) were tested at regular and saturating concentrations. The graphic on the right below shows the fluorescence intensity quantification. For each probe, no differences between the two conditions (t-test). These data indicate that the labelling of a subset of mitochondria by mTRIP is not due to limited concentrations of the probe. **(B)** Competition experiments between 40 ng of labelled probe ("lab", red) and increasing concentrations (0 ng, 40 ng and 200 ng) of unlabelled ("unlab", black) probe. Probes mTOT, mREP and mTRANS were tested. Below, fluorescence intensity quantification shows that, for each probe, the labelling is specific (reduction of the signal in the presence of increasing amounts of unlabelled probe). **(C)** Labelling (red) of probes mTOT, mREP and mTRANS is unaffected by the presence of probe TEL (5'TTAGGG repeats, green) that recognizes nuclear telomeric sequences. Below, fluorescence intensity quantification. T-test, no differences between the samples. **(D)** mTRIP signal is not affected by the probe size. Upper panel: schematic representation of the position of the probes (with the mitochondrial coordinates, see also Table S2) and of the genes present in the region tested; tRNAs are not represented. Mitochondrial coordinates according to MITOMAP (http://www.mitomap.org/MITOMAP). Middle panels: mTRIP labelling of HeLa cells with the indicated probes (red). Lower panel, fluorescence intensity quantification of 3D-reconstructed cells. The probe size is indicated on top. T-test, no differences between the samples. These data indicate that the probe size (200-1300 nt in length) does not affect the efficiency of FISH labelling. **(E)** 3D-reconstructed HeLa cells labeled with probe mTOTΔr, that consists in mTOT without probes that cover the mt ribosomal genes (probes 1, 2 and 14), untreated, and treated with RNaseA. Lower panel: fluorescence intensity quantification. t-test, compared to untreated cells. The intensity of labelling in the absence of rDNA probes is at least as high as with the probe mTOT (fluorescence intensity about 130k for mTOT, from in Fig. 1H), indicating that mTRIP labels mitochondrial mRNAs even in the presence of large amounts of rRNAs. Scale bars= 10 µm. Nuclei (blue) are labelled with Hoechst.

Figure S3. Mitochondrial network and mTRIP labelling in the presence and in the absence of nucleases. 3D-reconstructed HeLa cells labelled with probe mTOT (red), TOM22 immunolabelled (green), and merge, with or without nuclease(s) treatment (specified on the top of each panel; arrow indicates that second nuclease was added after 1h incubation with

first nuclease). mTOT labelling alone (in another set of cells) is shown in Fig. 1G. Scale bars= 10 μm.

Figure S4. Expression levels of the individual mitochondrial genes by RT-qPCR and additional analysis of specific *loci*. (A) Real-time quantitative PCR of individual mitochondrial genes in HeLa cells. 16S and 12S were analyzed with two independent sets of primers, (1) and (2). Expression level profiles of the mitochondrial genes are compatible with those observed by mTRIP analysis. Note that RT-qPCR detects transcripts of the entire mitochondrial and cellular populations whereas mTRIP reveals RNAs in a fraction of mitochondria and at the single-cell level. **(B)** Left panel: 3D-reconstructed HeLa cell with probe 14-1 that labels the 12S region (Table S2), scale bar= 10 μm. Right panel: fluorescence intensity quantification of probe 14-1. Data for probes 14 that labels 12S, and for probe 1 that labels 16S are from Fig. 2B and are shown for comparison. The size of the probes, in nucleotides, is indicated on the top of the column. These data show low mTRIP signal for *12S* with two independent sets of probes (14 and 14-1). Data from panels A-B are in agreement with the observation that, in spite mitochondrial RNAs are transcribed from a single molecule (essentially rRNAs from promoter P_{H1}, and mRNAs of the H-strand from promoter P_{H2} (Montoya et al, 1983, *Cell* 34: 151-9), different levels of individual RNAs are detected, compatibly with the turnover of the single transcripts (Gelfand and Attardi, 1981, *Mol. Cell. Biol.* 1: 497-511; Piechota et al., 2006, *Acta Biochim. Pol.* 53: 157-68). This is the case not only for mRNAs but also for 12S rRNA, which is detected here at lower levels than 16S rRNA (FISH and RT-qPCR experiments, for a total of seven loci examined), although similar levels of the two rRNAs were observed in vitro (Gelfand and Attardi, 1981, *cited*) and in vivo (Mercer et al., 2011, *Cell* 146: 645-658). Lower levels of 12S than 16S RNAs were nevertheless observed in several primary cells (Ninomiya and Ichinose, 2007, *PLoS One 2*: e1241; Welle et al., 1999, *Genome Res*. 9: 506-13), and the two rRNAs also appear differently sensitive to methylation (Cotney et al., 2009, *Hum. Mol. Genet*. 18: 2670-82; Metodiev et al., 2009, *Cell. Metab.* 9: 386-97) and to specific mitochondrial factors including ribosomes (Hyvarinen et al., 2010, *BMC Mol. Biol.* 11: 72; Smits et al., 2011, *Eur. J. Hum. Genet.*, 19: 394-9), indicating that lower levels of 12S versus 16S RNA detected with our analysis are compatible with reported physiological situations. **(C)** Left panel: 3D-reconstructed HeLa cell labelled with probe ND1, which recognizes a portion of the *ND1* gene (Table S2). Right panel: fluorescence intensity quantification of probe ND1 (and of probe 3, data from Fig. 2B, used as comparison) in presence and absence of nucleases. For each probe the coordinates in

the mitochondrial genome, and the target genes (in parenthesis), are indicated below. T-test, compared to untreated cells. Scale bars= 10 μm. The transcript levels of *ND1* (panel A) are compatible with the intensity of the mTRIP signal with the specific probe ND1 but not with probe 3, which labels additional genes, and probably also unterminated rRNA transcripts (see Fig. 3).

Figure S5. Colocalization of mTRIP labelling with mitochondria. (**A**) 3D-reconstructed HeLa cells labelled with the indicated mtDNA probe (red) and anti-TOM22 (green). Probes 1 (upper panels), 8 (middle panels), and 13 (lower panels) show high, low and intermediate colocalization levels with TOM22, respectively. **(B)** Percentage (p) of colabelling with mTRIP probes and anti-TOM22; n=30 cells; three independent experiments. A larger fraction of mitochondria carries *16S* RNA (probes 1-2), and *COII*, *ATP6*, *ATP8*, *COIII* RNAs (probes 6-7), than of the other mitochondrial transcripts. *COII* and *ATP6/8* have a longer half-live than the other transcripts in HeLa cells (Piechota et al., 2006, *Acta Biochim Pol* 53, 157-68). Probe 3 also shows high colocalization levels, but data in Fig. 3A,B indicate that this probe may also label unterminated rRNA transcripts. **(C)** Intensity of fluorescence in TOM22-labelled entities, calculated for each probe by multiplying the intensity of fluorescence of the probe (fi) by the percentage (p) of mTRIP labelled mitochondria (= fi x p). Each value indicates the relative amount of transcripts carried by the TOM22-labelled mitochondrial structures. Data in panels B and C indicate that not only *16S* RNA is present in a larger proportion of the mitochondrial population than are the other transcripts, but also that labelled mitochondria carry larger amounts of this than of the other transcripts. Conversely, the remaining transcripts are present in a small proportion of the mitochondrial population where they are also present in minor amounts. An intermediary situation was observed for the region of the mitochondrial genome that contains *COII* to *COIII* RNAs (probes 6-7), that are present in a large portion of mitochondria but in small amounts therein. Thus, 16S rRNA labels the large majority of mitochondria, and with an elevated signal per unit, whereas the other probes mainly identify distinct and in several cases minor mitochondrial fractions.

Figure S6. Immunofluorescence of nucleoid markers TFAM and Polγ with the mitochondrial marker TOM22. (A) Schematic representation of the position of probe mTRANS (mix of probes 1, 6 and 11), in red, on the human mitochondrial genome. **(B)** Colabelling of the nucleoid marker TFAM (red) with the mitochondrial marker TOM22 (green). Nucleus is stained by Hoechst (blue). Small panels on the right (magnification) show

large colocalization between the two markers (colocalization of TOM22 with TFAM: 99.94% ± 0.02%; n= 30 cells; three independent experiments). **(C)** Colabelling of the nucleoid marker Polγ (red) with the mitochondrial marker TOM22 (green). On the right, magnifications. Polγ is detected only in a fraction of mitochondria (colocalization of TOM22 with TFAM: 24.98% ± 1.87%; n= 30 cells; three independent experiments). Scale bars= 10 μm. **(D)** mTRIP labelling with mTRANS probe (red) and either anti-TFAM (green) or anti-Polγ (green), upper and lower panels, respectively. Panel on the right shows percentages of colocalization of marker on the X-axis with the marker indicated on the top of each column; n=30, three independent experiments**.** Note that TFAM and Polγ colocalized with mTRANS by 83.89 ± 4.7 % and by 92.69 ± 4.0 %, respectively, indicating that less than one tenth of the mitochondrial nucleoids labelled with these markers did not contain transcript levels detectable by this probe mix. Conversely, mTRANS colocalized by 63.53 ± 4.1% and by 66.23 ± 5.1 % with TFAM and Polγ, respectively, indicating that about one third of the mitochondrial transcripts revealed by this probe mix was not located in nucleoids where either TFAM or Polγ are present at detectable levels. The different extents of colocalization among foci are in agreement with significantly different amounts of TFAM in nucleoids (Chen and Butow, 2005, *Nat. Rev. Genet.* 6:815-25; Shutt et al, 2010, *PNAS USA*, 107: 12133-8; Spelbrink, 2010, *IUBMB Life* 1: 19-32; Wai et al., 2008, *Nat. Genet.* 40: 1484-8), and Polγ may be present at low or undetectable levels in transcription-active nucleoids. Therefore, within the limits of resolution of mTRIP, mTRANS largely colocalizes with nucleoid markers.

Figure S7. mREP labels initiation of mtDNA replication. (A) 3D-reconstructed HeLa cells labelled with probe mREP (red) and anti-BrdU (green) at different times of exposure to 10 μm BrdU. Nuclei are labelled by Hoechst (blue). mTRIP was performed followed by BrdU immunostaining. Scale bar=10 μm. **(B)** Fluorescence intensity quantification. Left panel, BrdU; right panel, mREP (white), and proportion of mREP that colocalizes with BrdU (black); n=30, three independent experiments. Time 18h was tested in seven independent experiments. **(C)** Schematic representation of BrdU and mREP labelling patterns. mREP+ signal (red) results from hybridization of the probe to the corresponding DNA sequence (within an accessible structure). The O_H origin is schematically represented with a purple square. BrdU labelling is indicated with green spots along the newly synthesized mtDNA chain. A number of green spots below threshold results in $BrdU^-$ signal. Open mtDNA at O_H

without DNA synthesis (standby position) also results in $BrdU^-$ signal. BrdU incorporation distant from the origin O_H is not compatible with mREP labelling (inaccessible DNA structure). **(D)** Detail of 3D-reconstructed cells (2.5x magnification) labelled with mREP (red), anti-BrdU (green), and merge; nuclei are labelled by Hoechst (blue) at 18h exposure to BrdU. Two regions, proximal and distal to the nuclear surface are shown in upper and lower panels, respectively. In lower panels, circles indicate representative mREP-positive and mREP-negative areas, where BrdU labelling was also measured. On the right, fluorescence intensity measurement of BrdU labelling shows higher values in mREP-negative than in mREP-positive areas. n=300 areas, three independent experiments. Scale bar= 4μm. **(E)** mREP anticipates the increases in mtDNA content. Cells were treated with 50 μM of H_2O_2 which increases the mtDNA content (Lee et al, 2005, *Ann. NY Acad. Sci.* 1042:246-54). Fluorescence intensity quantifications of mREP, left panel; and mtDNA content estimation by qPCR (12S region), right panel. Ctrl, untreated; 1h to 24h, time in the presence of H_2O_2. n=3. T-test, compared to untreated cells. mREP labelling increase by about 70% 1h after H_2O_2 treatment, when the DNA content is low, and returned to control values 3h after treatment when the original mtDNA content was restored compatibly with the time necessary to replicate the mt genome (about 92 minutes for total mtDNA replication (Korhonen et al, 2004, *EMBO J.* 23: 2423-9)). **(F)** Upper panel, scheme of primers for the estimation of 7S DNA and mtDNA content by real-time qPCR as described (Antes et al., 2010, *Nucleic Acids Res.* 38:6466-76). 7S DNA corresponds to amplification of AB1; mtDNA corresponds amplification of AB2-AB1. Lower panel**,** cells treated with H_2O_2 as in panel E. 7S (white columns) and mtDNA (grey columns) content. The small panel on the right represents values on a scale adapted to detect the variations of mtDNA (grey columns). n=3 independent experiments. T-test, compared to untreated cells (ctrl); black stars for mtDNA, grey stars for 7S; Scale bar =10 μm.

Figure S8. Heterogeneity of nucleic acid composition in large foci at the replication origin O_H and in the 7S region (A) Enumeration of large PL-OH (green) and 7S (red) foci. The number in parenthesis represents the corresponding labelling pattern (numbered as in Fig. 5B). Pattern numbers common to PL-OH and 7S large foci are in white. Pattern numbers specific to 7S foci are in black, and in this case the proportion of events is indicated with a brace. Foci in sample treated simultaneously with DNaseI and RNAseH are smaller than in the other samples. T-test: 7S versus PL-OH foci; ns, not significant. **(B)** Scheme of nucleic acids detected in large PL-OH and 7S foci (a/o= and/or; RHR-RNA/DNA=RNaseH resistant

RNA/DNA hybrids), with the pattern number indicated on the right.

Taken together, panels A and B, as well as Fig. 5B reveal the following nucleic acid compositions. Pattern 1: about one half of large PL-OH foci are DNaseI-resistant and RNaseH-sensitive, and they essentially colocalize with foci of the downstream 7S probe. Differently from PL-OH, however, large 7S foci are essentially RNaseH-resistant. Thus, these large PL-OH and 7S foci colocalize but the former probe recognizes RNA/DNA hybrids whereas the latter recognizes RNA. Pattern 1 large foci are thus compatible with transcripts bound to the DNA template proximally to the promoter (probe PL-OH), and of single-strand RNA distally from the promoter (probe 7S). Given the direction of transcription, these nucleic acids are unlikely associated with a single transcription event. Pattern 5: most of the other half of large DNAseI-resistant PL-OH and 7S foci are RNaseH-resistant, and therefore consist of either RNAseH-resistant RNA/DNA hybrids (possibly R-loops) or of RNA. Given that about one half of PL-OH and 7S foci are also RNaseA-sensitive, and that combined RNAseA and RNAseH treatment erases most PL-OH foci, it is likely that pattern 5 corresponds to RNA at both PL-OH and 7S locations (Fig. 5D). Pattern 3: large DNaseI-resistant 7S foci and apparently DNaseI-sensitive PL-OH foci indicate accessible DNA structure at PL-OH whereas RNA (as single strand or as RNA/DNA hybrid) is present at the level of 7S. The frequency of foci in pattern 3 was not determined with significant accuracy given the low number of foci/cell, although they may account for about 15% of 7S large foci (see panel A). Pattern 4: RNaseA-resistant PL-OH and 7S foci were observed which indicate no free L-strand transcript at either position. The almost equivalent number of RNaseA-resistant and RNAseH-sensitive PL-OH foci, as well as the disappearance of foci after combined treatment with RNaseA and RNaseH, suggest that pattern 4 corresponds to RNA/DNA hybrids at PL-OH. Given the direction of transcription, the nucleic acids in pattern 4 are also unlikely associated with a single transcription event. Pattern 6: DNA in the 7S region, and no labelling in the PL-OH region. Pattern 6 reveals rare foci with exclusive DNA labelling in the 7S region, and no labelling in the PL-OH region. Interestingly, treatment with DNAseI slightly increased the number of PL-OH and 7S foci, indicating that DNA masks some RNA targets at both loci, compatibly with the presence of structured nucleic acids which also contains DNA in this region.

Figure S9. mREP and BrdU labelling in normal and *Rrm2B* fibroblasts. 3D-reconstructed fibroblasts labelled with mREP (red) and anti-BrdU (green) after 30 min, 3h and 18h treatment with BrdU. Merge images are as in Fig. 7E. Scale bar= 10 μm.

RT-qPCR primers

Probe	forward primer	reverse primer	reference
TBP	CTCACAGGTCAAAGGTTTAC	GCTGAGGTTGCAGGAATTGA	*Mercy et al. 2005. FEBS Journal 272(19):*
12S (1)	CTGCTCGCCAGAACACTACG	TGAGCAAGAGGTGGTGAGGT	*Suissa et al. 2009. PLoS Genetics 5(5):e1000474*
12S (2)	AAACTGCTCGCCAGAACACT	CATGGGCTACACCTTGACCT	*Uchuimi et al. 2010. NAR 38(16)*
16S (1)	GTATGAATGGCTCCACGAGG	GGTCTTCTCGTCTTGCTGTG	*Suissa et al. 2009. PLoS Genetics 5(5):e1000474*
16S(2)	GCTAAACCTAGCCCCAAACC	TTGGCTCTCCTTGCAAAGTT	*Uchuimi et al. 2010. NAR 38(16)*
ND1	TGGCCAACCTCCTACTCCTC	ATGGCGTCAGCGAAGGGTTG	*Suissa et al. 2009. PLoS Genetics 5(5):e1000474*
ND2	ACTGCGCTAAGCTCGCACTG	ATTATGGATGCGGTTGCTTG	*Suissa et al. 2009. PLoS Genetics 5(5):e1000474*
COI	ACCCTAGACCAAACCTACGC	TAGGCCGAGAAAGTGTTGTG	*Suissa et al. 2009. PLoS Genetics 5(5):e1000474*
COII	ACAGATGCAATTCCCGGACG	GGCATGAAACTGTGGTTTGC	*Suissa et al. 2009. PLoS Genetics 5(5):e1000474*
ATP8	ATGCCCCAACTAAATACT	TTGTGGGGGCAATGAATG	*Uchuimi et al. 2010. NAR 38(16)*
ATP6	CCCACTTCTTACCACAAGGC	GTAGGTGGCCTGCAGTAATG	*Suissa et al. 2009. PLoS Genetics 5(5):e1000474*
COIII	ACTTCCACTCCATAACGCTC	TGGCCTTGGTATGTGCTTTC	*Suissa et al. 2009. PLoS Genetics 5(5):e1000474*
ND3	CTACCATGAGCCCTACAAAC	ACTCATAGGCCAGACTTAGG	*Suissa et al. 2009. PLoS Genetics 5(5):e1000474*
ND4L	TATCGCTCACACCTCATATC	AGGCGGCAAAGACTAGTATG	*Suissa et al. 2009. PLoS Genetics 5(5):e1000474*
ND4	ACAAGCTCCATCTGCCTACG	TTATGAGAATGACTGCGCCG	*Suissa et al. 2009. PLoS Genetics 5(5):e1000474*
ND5	GGTTTCATCCTCGCCTTAGC	ACCTAATTGGGCTGATTTGC	*Suissa et al. 2009. PLoS Genetics 5(5):e1000474*
CYTB	CTCCCGTGAGGCCAAATATC	GAATCGTGTGAGGGTGGGAC	*Suissa et al. 2009. PLoS Genetics 5(5):e1000474*
ND6	ATTGGTGCTGTGGGTGAAAG	GGATCCTCCCGAATCAACCC	*Suissa et al. 2009. PLoS Genetics 5(5):e1000474*
NRF1	GGAGTGATGTCCGCACAGAA	CGCTGTTAAGCGCCATAGTG	*Savagner et al. 2003. Biochem Biophys Res Com310(3)*

qPCR primers

Probe	forward primer	reverse primer	reference
18S	GAGAAACGGCTACCACATCC	GCCTCGAAAGAGTCCTGTAT	*Suissa et al. 2009. PLoS Genetics 5(5):e1000474*
12S	GCTCGCCAGAACACTACGAG	CAGGGTTTGCTGAAGATGGC	*Parone et al. 2008. PLoS One 3(9):e3257*
A	GTGGCTTTGGAGTTGCAGTT	-	*Antes et al. 2011. NAR 38(19):6466-6476*
B1	-	CAGCCACCATGAATATTGTAC	*Antes et al. 2011. NAR 38(19):6466-6476*
B2	-	GAAGCAGATTTGGGTACCAC	*Antes et al. 2011. NAR 38(19):6466-6476*

Table S1. RT-qPCR and qPCR primers. The sequence of forward and reverse primers for RT-qPCR (upper panel) and qPCR (lower panel) is indicated after the name of the probe that also indicats the gene analysed. Number in parenthesis indicate different sets used to test the same gene. The pair A-B1 amplifies a mtDNA region included in 7S, while the pair A-B2 amplifies a region beyond 7S in the direction of the H-strand (see scheme in Supplementary Figure S6D). Reference is indicated in the last column.

Probe	start	end	size
14-1	650	1598	949
ND1	3515	3715	200
ATP8	8366	8566	200

mTOTΔr	probes 3 to 13 (rRNA probes excluded)

Table S2. Coordinates of additional probes used in this study. The start and end points of probes used for FISH experiments are given on the mitochondrial DNA (NC_012920, GenBank). mTOTΔr, which is a mix of eleven probes is indicated below.